fluids

MDPI

Article

Filaments, Fronts and Eddies in the Cabo Frio Coastal Upwelling System, Brazil

Paulo H. R. Calil [1,*], Nobuhiro Suzuki [1], Burkard Baschek [1] and Ilson C. A. da Silveira [2]

[1] Institute of Coastal Ocean Dynamics, Helmholtz-Zentrum Geesthacht, 21502 Geesthacht, Germany; nobuhiro.suzuki@hzg.de (N.S.); burkard.baschek@hzg.de (B.B.)
[2] Instituto Oceanográfico, Universidade de São Paulo, São Paulo 05508-120, Brazil; Ilson.silveira@usp.br
* Correspondence: paulo.calil@hzg.de

Abstract: We investigate the dynamics of meso- and submesoscale features of the northern South Brazil Bight shelf region with a 500-m horizontal resolution regional model. We focus on the Cabo Frio upwelling center, where nutrient-rich, coastal waters are transported into the mid- and outer shelf, because of its importance for local and remote productivity. The Cabo Frio upwelling center undergoes an upwelling phase, from late September to March, and a relaxation phase, from April to early September. During the upwelling phase, an intense front around 200 km long and 20 km wide with horizontal temperature gradients as large as 8 °C over less than 10 km develops. A surface-intensified frontal jet of 0.7 ms^{-1} in the upper 20 m and velocities of around 0.3 ms^{-1} reaching down to 65 m depth makes this front a preferential cross-shelf transport pathway. Large vertical mixing and vertical velocities are observed within the frontal region. The front is associated with strong cyclonic vorticity and strong variance in relative vorticity, frequently with $\mathcal{O}(1)$ Rossby numbers. The dynamical balance within the front is between the pressure gradient, Coriolis and vertical mixing terms, which are induced both by the winds, during the upwelling season, and by the geostrophic frontal jet. Therefore, the frontal dynamics may be largely described as sum of Ekman and turbulent thermal wind balances. During the upwelling phase, a mix of barotropic and baroclinic instabilities dominates in the upwelling center. However, these instabilities do not lead to the local formation of coherent eddies when the front is strong. In the relaxation phase, the front vanishes, and the water column becomes less stratified. The interaction between eastward coastal currents generated by sea level variability, coastal intrusions of the Brazil Current, and sporadic wind-driven, coastal upwelling events induce the formation of cyclonic eddies with diameters of, approximately, 20 km. They are in gradient-wind balance and propagate along the 100-m isobath on the shelf. During this phase baroclinic instability dominates. Cold filaments with widths of 2 km are formed due to straining and stretching of cold, coastal temperature anomalies. They last for a few days and are characterized by downwelling as large as 1 cms^{-1}. The turbulent thermal wind balance provides a good first order estimate of the dynamical balance within the filament, but vertical and horizontal advection are shown to be important. To our knowledge, this is the first account of these smaller scale features in the region. Because these meso- and submesoscale features on the shelf heavily affect the water properties crucial to productivity of the South Brazil Bight, it is important to take these features into account for a better understanding of the functioning of this ecosystem and its resilience to both direct human activities as well as to climate change.

Keywords: coastal upwelling; continental shelf; western boundary current; Brazil Current; mesoscale dynamics; submesoscale dynamics

Citation: Calil, P.H.R.; Suzuki, N.; Baschek, B.; da Silveira, I.C.A. Filaments, Fronts and Eddies in the Cabo Frio Coastal Upwelling System, Brazil. *Fluids* **2021**, *6*, 54. https://doi.org/10.3390/fluids6020054

Academic Editor: Jonathan Gula
Received: 14 December 2020
Accepted: 1 January 2021
Published: 25 January 2021

1. Introduction

The South Brazil Bight (SBB) is adjacent to the most densely populated area of the Brazilian coast. Economical activities on the shelf region and offshore include, among others, tourism, fisheries, oil and gas exploration and navigation. This puts significant pressure

on the ecosystem services provided by the ocean and requires a thorough understanding of the functioning of the marine environment. This will guide conservation efforts, help mitigate the human impact on the ocean. and provide sustainable development under the likely consequences of a changing climate.

Relevant processes associated with ecology, marine conservation, and protection include wastewater and oil dispersal, larval transport and connectivity, phytoplankton productivity, and cross-shelf exchange. They largely depend on physical processes that occur on spatial scales of hundreds of meters to a few kilometers which are usually not resolved either by traditional observational sampling or by global and even regional model simulations.

Coastal and shelf regions are strongly sensitive to spatially variable forcing such as winds and smaller-scale topographic features. Observational studies in coastal upwelling regions estimate shear-induced convergence as large as f, the Coriolis parameter, within small scale fronts [1,2]. This would lead to the accumulation of surface debris and/or organic material resultant from surface productivity and affect the rate of particle export [3], thus modulating phytoplankton distribution, species composition, and the supply of organic material to benthic communities. Coastal eddies with radii of 4–15 km and a life span of 2–6 days are thought to impact nutrient delivery and organic matter export [4]. This is comparable to the radius of deformation on the shelf, $R_d = \frac{Nh}{f}$, where N is the averaged buoyancy frequency in a water column of depth h and f is the Coriolis parameter. Using average values for the region yield $R_d \approx 15$ km. The radius of deformation is the horizontal scale of mesoscale eddies in the ocean while the typical length-scales for submesoscale motions is around $\frac{R_d}{10}$ [5,6]. Therefore, coastal eddies and fronts are the transition between meso- and submesoscale motions. Their interaction with sheared coastal currents may lead to the formation of filaments, which are extrema in surface density, thinner and more episodic than fronts, and are associated with very strong downwelling [7]. Eddy-filament systems have been shown to affect the distribution and transport of dissolved and particulate organic carbon in the north-western Africa upwelling system [8].

Previous modeling studies have shown that as horizontal resolution is increased, energetic submesoscale processes emerge, and are associated with ageostrophic motions on spatial scales of one kilometer or less and temporal scales of one day or less [5,6,9]. In the open ocean, both numerical simulations and in-situ observations have in the last two decades shown the importance of these motions to both the dynamics and the biogeochemistry of the upper ocean. This has potential consequences for long-term climate predictions primarily due to the restratification induced by mixed layer instabilities [10]. Nearshore and on the continental shelf, high-resolution, surface observations [11–13] and submesoscale-resolving model simulations [14,15] have recently shown the importance of coastal submesoscale fronts, filaments, and eddies on transport properties and dynamics of these regions.

The SBB is a region with considerable overlap between shelf and open-ocean dynamics. The southward-flowing Brazil Current (BC) follows the shelfbreak as it abruptly veers eastward at around 23° S. The change in coastline orientation induces meandering of the BC and the occasional generation of mesoscale eddies which often occupy a portion of the shelf [16]. These eddies affect the circulation on the outer shelf below the surface, by modulating intrusions of South Atlantic Central Water (SACW) onto the shelf, while helping export coastal surface waters from the upwelling center offshore (Figure 1).

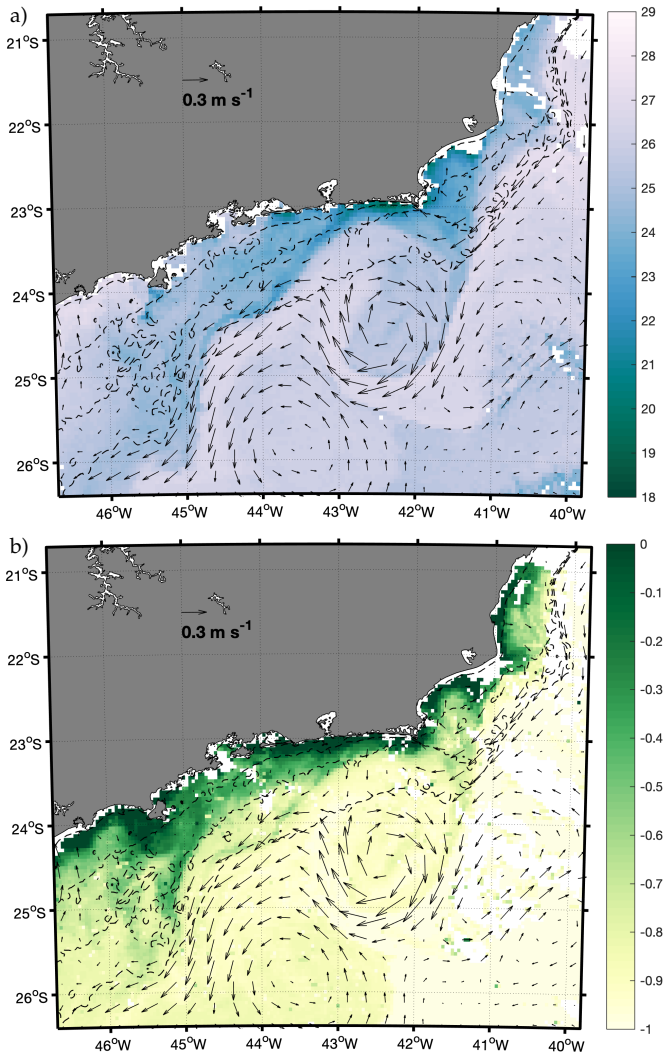

Figure 1. (**a**) Sea Surface Temperature (in °C) obtained by the AVHRR-15, Level 3 product and surface geostrophic velocoties from AVISO on 25 April 2002. (**b**) Surface chlorophyll (in $\log_{10}$ (kg m^3)) for 25 April 2002 obtained by the SeaWIFS product. Dashed lines show the isobaths of 10 m, 50 m, 100 m, and 200 m.

Northeasterly winds primarily force the Cabo Frio (CF) coastal upwelling center during summer months [17,18]. In-situ observations collected during the DEPROAS Experiment [19–21] in the summer of 2001 and 2002 show the vertical and horizontal structure of the upwelling front off Cabo Frio (Figure 2). While the horizontal resolution of CTD stations does not resolve submesoscale features, it shows the strong horizontal gradients in temperature and density over a distance of around 10 km. Figure 2a shows the upwelling front during the summer of 2001 just off Cape Frio with a surface temperature varying from 15 °C to 25 °C within 20 km from the coast. Colder waters from the oceanic seasonal and permanent pycnoclines upwell nearshore. Figure 2b depicts the horizontal distribution of the upwelling front during the summer of 2002 when the plume occupied at least 250 km of the inner shelf just west of Cabo Frio with minimum temperatures of around 15 °C nearshore. In addition to the wind-driven upwelling front, coastal currents may be induced by sea level variability due to local winds or remote forcing, such as continental shelf waves [22,23]. As the coastal upwelling center off CF interacts with coastal currents and the BC eddies and meanders, a front is generated with a width of $\mathcal{O}$(1–10) km and stretches for tens to hundreds of kilometers southwestward along the SBB shelf [24]. In fact, sea surface temperature (SST) images (Figure 1a) suggest a preferential pathway of cross-shelf transport probably arising as a consequence of the interaction

between the wind-driven upwelling center, coastal currents, and intrusions of the BC. This leads to the horizontal advection of recently upwelled, coastal, and nutrient-rich waters along this front to the mid-shelf, thereby affecting biological productivity of the shelf region, as suggested by Figure 1b. These images show that colder waters from the CF upwelling center occupy a large portion of the northern SBB shelf and are preferentially advected southwestward along the front. This elongated front on the shelf seems to be formed by a combination of the effect of the open-ocean cyclonic eddy on the shelf and coastal currents which squeeze and eject cold waters southwestward from the coast all the way to the 200-m isobath. The chlorophyll-a image (Figure 1b) shows a filament of high chlorophyl aligned with the upwelling front showing that the front advects high-biomass waters from the coastal region into the mid- and outer shelf. Cross-shelf transport is also directly induced by the open ocean cyclonic eddy as it engulfs coastal waters at its northeastern side and advects them offshore. This is also seen in the chlorophyll-a image, where coastal waters with higher chlorophyll concentration are transported offshore, spiraling into the cyclonic eddy. Also note the headland wake that is formed near São Sebastião island at around 45.4° W, 24° S, which suggests the existence of secondary upwelling centers in the region which, to the authors' knowledge, has not been previously reported.

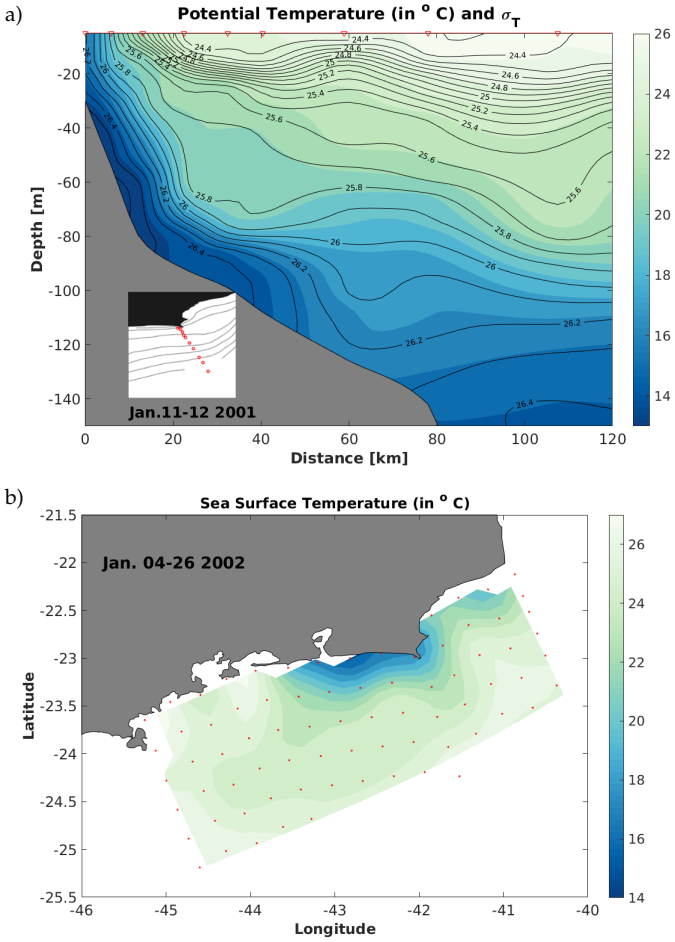

Figure 2. The Cape Frio upwelling front from the DEPROAS Experiment conducted aboard R/V Prof. W. Besnard of the Oceanographic Institute of the University of São Paulo. (**a**) The front vertical structure sampled in the summer of 2001. The red triangles represent the position of each CTD station, which were spaced from about 5 km in the inner portion of the transect to 20 km over the shelf break. (**b**) The front horizontal distribution of the upwelling front during the summer of 2002. The red dots represent the location of the CTD stations, which were on average spaced 15 km from each other.

The interaction between the upwelling center—located between 42° W and 43° W, 23° S—with sheared currents can potentially give rise to a wealth of smaller scale processes. In the adjacent open ocean, a number of recent studies has shown the importance of submesoscale dynamics on the BC system and its interaction with bathymetric features [25–27]. On the shelf, however, despite the potential importance of submesoscale motions and fronts for the ecosystem of the SBB, knowledge about the local dynamics is based on climatological estimates from historical records [23,28], point-wise time-series over specific periods [29], and mesoscale-resolving observational studies or numerical simulations [16]. While these more commonly studied mesoscale motions are important components of the local circulation and act as modulators of the intrusions of the nutrient-rich SACW onto the outer shelf [30], there are indications that the neglected smaller scale processes may play an important role in explaining the productivity on the SBB shelf.

In this study, we use a 500-m resolution regional model whose domain encompasses both the shelf and open ocean region in order to explore the occurrence of submesoscale features and their importance on the shelf, shelfbreak, and adjacent open ocean in the SBB. We focus on three specific features that are commonly observed in the region, namely, coastal eddies generated by headlands, the CF coastal upwelling front, and cold filaments that arise as cold temperature anomalies are squeezed due to convergent flow.

2. Methods

We use the Coastal and Regional Ocean Community Model (CROCO) at a horizontal resolution of 500 m and 50 sigma vertical levels, with stretching parameters chosen (θ_s = 7.0, θ_b = 2.0 and Tcline = 300) so that higher vertical resolution in the upper ocean is attained. The model is forced with daily surface wind stress from QuikSCAT for the year 2003 and climatological heat fluxes from COADS. At the three open boundaries, we use the Simple Ocean Data Assimilation reanalysis, version 3.3.1 [31] with a 5-day temporal resolution for the year 2003. Barotropic tides from TPX07 [32] are added to the forcing. The horizontal and vertical advection schemes used for tracers and momentum are the 5-th order weighted essentially nonoscillatory scheme (WENO5). Vertical mixing is parameterized with the k-profile parameterization (KPP), both in the surface and bottom boundary layers [33] which has been shown to be suitable for coastal applications [34].

We chose the 500 m horizontal resolution as an optimal compromise between domain size and horizontal resolution in a dynamically consistent model domain that allows the simulation of the open ocean dynamics, its connection to the shelf, the boundary current system along the shelfbreak, as well as the shelf dynamics. This study should be considered as a lower bound estimate for the importance of the submesoscale on the shelf region. At higher spatial resolution (e.g., $\mathcal{O}$ (10 m)), not only some of the processes observed would be fully resolved but other processes would emerge as shown by recent modeling work in other coastal regions [15]. Because of the highly advective nature of the fronts, filaments, and coastal eddies, a nested approach with a small domain in the region of interest would probably not allow the full evolution of submesoscale structures that are advected over relatively large distances.

Our model simulation was spun up starting from 1 Jan. 2003 of the SODA reanalysis and repeating the same cycle for three years. All results in this work are based on daily averages of the 4th year of the model run. Despite the ephemeral nature of submesoscale features such as fronts, eddies, and filaments, we focus on those which were robust enough to persist for at least one day and investigate the averaged effect of these processes on a daily basis. Instantaneous snapshots of specific variables yield a myriad of smaller scale patterns whose detailed analysis is out of the scope of the present study. We discuss potential implications of these motions in Section 4.

3. Results

3.1. Overview and Observational Motivation

We focus on the northern part of the SBB and how shelf and open ocean currents interact with the most prominent oceanographic feature of the region, namely the the coastal upwelling center off CF (Figure 1). The primary forcing mechanism of the coastal upwelling are the northeasterly winds which blow in the area during the upwelling phase, from late September to March. During the relaxation phase, from April to late August winds subside and occasionally reverse, alternating episodes of coastal upwelling and downwelling but with less intensity than during the upwelling phase. The relaxation phase in 2003 started at around day 70 (mid March) and lasted until day 200 (end of July), when larger peaks in Ekman pumping start to occur at higher frequency (Figure 3(top)). Sea level at the coast is strongly influenced by the local winds but there is considerable low-frequency variability which could be due to continental shelf waves, which are known to occur in the region [22], or large-scale variability (Figure 3(middle)). The relaxation phase in this year coincides with a period when net heat flux decreases and becomes negative (from days 160 to 220) which, together with the reduced upwelling-favorable winds, leads to a less stratified water column because of the reduced intrusion of SACW from below. Figure 3(bottom) shows the net heat flux from the climatological COADS product and Ekman pumping calculated from the QuikSCAT winds for 2003, both box-averaged over the Cape Frio coastal upwelling center (the green rectangle in Figure A1). The distinction between the upwelling and relaxation phase is clear, as the winds subside, Ekman pumping decreases. This is the season when the net heat flux also decreases, thus favoring mixing and a more uniform water column, as opposed to the two-layered system during the upwelling season.

Remotely-sensed products clearly lack the spatial and temporal resolution to provide sufficient detail on the generation and evolution of fronts and eddies on the shelf and near the coast. SST and chlorophyll-a images do suggest, however, that the interaction between the coastal upwelling center and strongly sheared currents leads to the formation of filaments, coastal eddies, and continental shelf fronts. In addition, satellite imagery provides anecdotal evidence for some of the processes analyzed in detail in our model solutions. Specifically, we selected three dates with relatively clear images in 2003, the same year of the model run, where a coastal eddy, a filament, and a front were detected. Figure 4a shows a recently-formed, cold anomaly at 42° W, between the 50-m and 100-m isobaths, just southwest off CF on 23 May 2003, during the relaxation phase, when the winds and heat fluxes are reduced the water column near the coast is less stratified than during the upwelling phase, when strong winds bring colder waters near the coast thus maintaining a largely two-layered system. The coastal eddies have diameters of a few tens of kilometers and seem to be formed by instabilities caused by sheared currents near the region of coastline veering. Although not much can be said from the AVISO velocities on the shelf, the coastal jet may interact with coastal currents induced by the propagation of continental shelf waves, which are most intense in the fall/winter due to atmospheric forcing [22].

Figure 4b shows a cold filament on 10 September 2003 extending from the coast to the mid-shelf, between the 100-m and 200-m isobaths. This filament was formed after a strong wind burst in the region (day 250 on Figure 3(top)). Our model results show the evolution of a feature that is very similar to this one (Section 3.3). Figure 4c shows a more developed upwelling center with colder temperatures near the coast on 21 December 2003 and what looks like an ejection of a cold filament advected southwestward by a coastal branch of the BC, as seen from the AVISO velocities.

The examples shown in Figure 4, namely a cold eddy at the end of May 2003, a filament in September 2003 and the upwelling front in December, coincidentally look very similar to modeled results around the same dates. We stress, however, that we did not attempt to simulate observed features with our 500-m model simulation. Instead, we explored the simulation for phenomenological discovery of processes that have, to our knowledge, not been reported before. This coincidence shows the importance of local, synoptic wind

forcing for the processes observed on the shelf. We explore the dynamics of these features in the following sections. A brief validation of our model run is shown in the Appendix A.

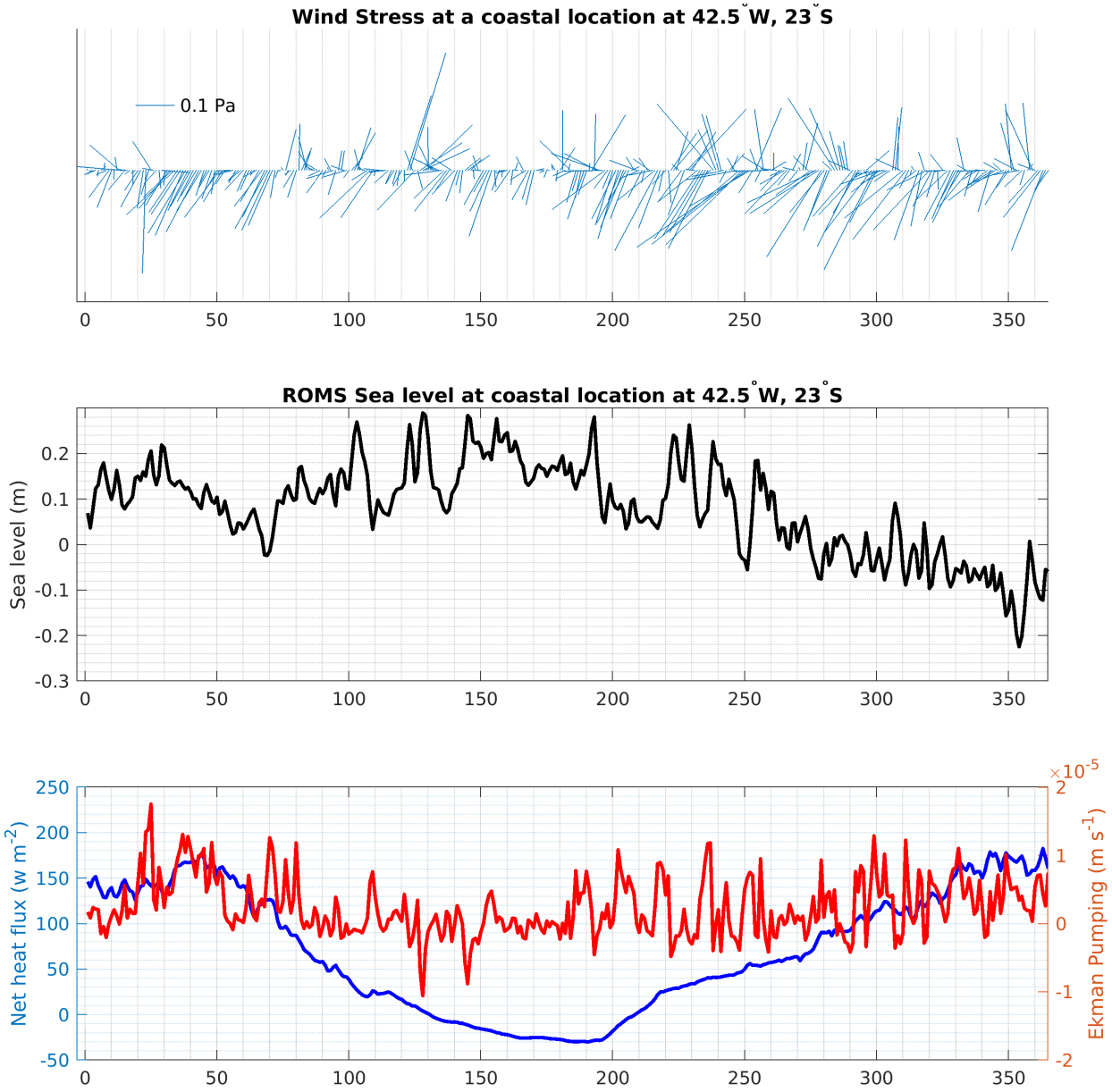

Figure 3. (**Top**) Stickplot of the wind stress magnitude and direction (positive northward) from QuikSCAT, used to force the model, for 2003 at a coastal location at the Cabo Frio upwelling center. (**Middle**) Time-series of the ROMS Sea level at the same location. (**Bottom**) Box-averaged net heat flux and Ekman pumping over the Cape Frio upwelling region (See Figure A1). Vertical blue lines mark the beginning and end of the relaxation phase on days 72 and 185, respectively.

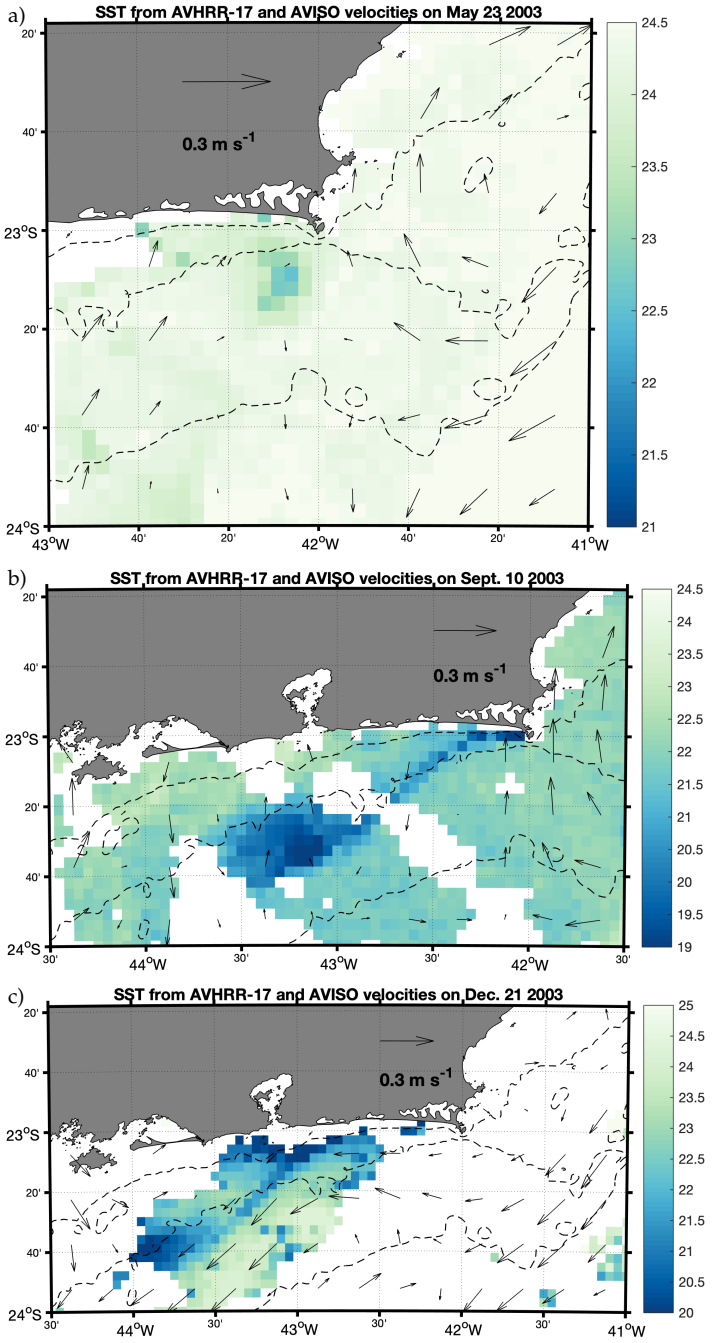

Figure 4. (**a**) SST (in °C) from AVHRR-17 and surface geostrophic velocities from AVISO on 23 May 2003 showing a coastal cyclonic eddy recently formed just off Cabo Frio. The size of the eddy and the timing of its formation is similar to the modeled eddy shown in Section 3.2.3. (**b**) SST and surface geostrophic velocities on 10 September 2003 showing a coastal filament. (**c**) SST and surface geostrophic velocities on 21 December 2003 showing the coastal upwelling center off Cabo Frio. Dashed lines show the isobaths of 50 m, 100 m, and 200 m.

3.2. Meso- and Submesoscale Activity in the CF Upwelling Center

In order to identify regions prone to the emergence of submesoscale processes, we calculate the mean, variance, and the skewness of the local Rossby number, $Ro = \frac{\zeta}{f}$, where ζ is the surface relative vorticity and f is the Coriolis parameter. The variance and skewness of surface divergence are normalized by the absolute value of the Coriolis parameter (Figure 5). Overall, we see that large cyclonic vorticity is associated with the region where the upwelling front separates from the coast. There are significant deviations

from the mean state, as seen from the large variance of *Ro* and the negative skewness of the horizontal divergence. It shows that that nonlinearity and ageostrophy, typical of submesoscale fronts and filaments, is important [15,35].

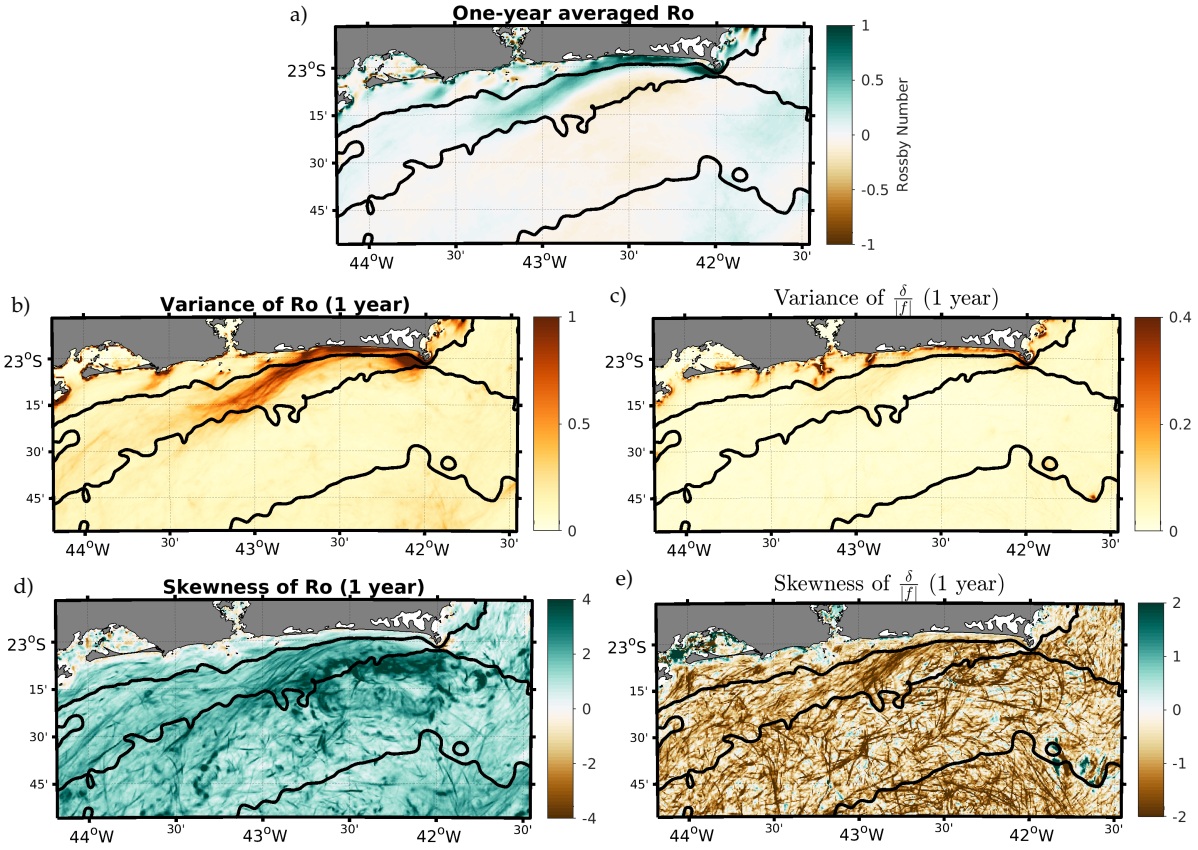

Figure 5. Annual mean (**a**), variance (**b**) and skewness (**d**) of the local Rossby number. Variance (**c**) and skewness (**e**) of the horizontal divergence. All metrics are calculated from 365 daily averages of the modeled horizontal velocities for 2003.

Figure 5 indicates different dynamical regions within the coastal upwelling center. Just west of Cape Frio, between the isobaths of 50-m and 100-m, we find large vorticity variance, low vorticity skewness, and low divergence variance and skewness. A similar pattern is seen in the coastal region shoreward of the 50-m isobath. This suggests that these regions are consistently forming strong cyclonic vorticity which is largely in geostrophic balance. The first region is a place of abrupt change in coastline orientation and isobath convergence. The second one is the region where the coastal jet flows to the west.

Along the 100-m isobath, we see low variance and large skewness of relative vorticity, as well as relatively large skewness in horizontal divergence. This suggests that this is a region of sporadic but robust cyclonic vorticity events which are mostly, but not completely, in geostrophic balance. As will be seen in the next sections, these cyclonic eddies have diameters of a few tens of kilometers, are preferentially formed in the relaxation phase when the upwelling front is weak or nonexistent and may either propagate coherently across the shelf or be ejected into the open ocean depending on specific conditions during their formation.

Thirdly, we see a high variance of the local Rossby number in the region where waters from the coastal upwelling center are preferentially advected across the shelf over a few hundred kilometers, from the coast to the 100-m isobath. This is the location of a semipermanent front, which is intensified during the upwelling phase. It is associated with strong convergence as seen from negative values of the skewness of the horizontal divergence (Figure 5e). While the location of the front is relatively fixed, as seen from the average Rossby number, the variance around the mean is also large (Figure 5a,b). The front

(see Section 3.2.1) vanishes in the relaxation phase, but episodic upwelling events form weaker, more episodic fronts at approximately the same location (see Section 3.3).

As discussed above, the dimensions of the front and coastal eddies are similar to the deformation radius on the shelf which makes these features largely mesoscale. However, the strong ageostrophy and nonlinearity associated with them frequently gives rise to submesoscale features such as cold filaments, formed when cold temperature anomalies, usually generated by coastal upwelling, are stretched and squeezed thereby intensifying existing horizontal density gradients. As a consequence, cross-filament, counter-rotating, ageostrophic secondary circulations (ASC's) develop on each side of the filament resulting in very large downwelling due to the sum of downwelling component on each counter-rotating ASC [7,36,37] (See Section 3.2.2). They are ephemeral, but intense features whose existence may be reflected on the large values of skewness of relative vorticity and convergence throughout the shelf.

Based on the one year model simulation, we can characterize the region as front-dominated, during the upwelling phase, where the local formation of coastal eddies is hindered and as eddy-dominated, during the relaxation phase, when the front is weaker or nonexistent and coherent eddies develop locally. These features are important both from a dynamical and biogeochemical point of view. In the remainder of this paper we explore them in more detail. We will discuss their implications in Section 4.

3.2.1. The CF Upwelling Front

Figure 6a shows modeled SST for 17 December 2003 and gives a general idea of the conditions during the upwelling season in the northern part of the SBB. While we will focus on features that are formed in the vicinity of the CF upwelling center, it is worth noting that there are smaller, localized regions of increased upwelling along the coast. In particular, we note the region in the lee of the Island of São Sebastião (45.5° W, 23.8° S) between the 10 m and 50 m isobaths. The observed SST shown in Figure 1a confirms the existence of this secondary upwelling center, which is independent of the CF upwelling center and is formed due to interactions between the coastal flow and the island/headland. To our knowledge, this has not been reported before. Although localized and somewhat restricted to the inner shelf, it may help explain local productivity patterns.

During the upwelling phase, an intense front develops in the northern SBB (Figure 6a). This is a dominant feature of the region, as seen from the mean and variance of the relative vorticity (Figure 5). It is a preferential pathway for water transport from the coastal upwelling center into the wider continental shelf to the southwest. Note the similarity, in terms of location of the front, with the observed SST pattern shown in Figure 4c. Modeled SST is colder than the one obtained by remote-sensing, which is to be expected given the positive bias, as large as 4 °C during the upwelling season, recently observed in remotely-sensed products when compared to observations in the region [38]. The horizontal temperature gradient within the front is approximately 8 °C over a distance of less than 10 km. The frontal jet flows from the coast southwestward at a bearing of around 065° all the way to the 100-m isobath. A cross-frontal transect taken along the green line in Figure 6a reveals a surface-intensified frontal jet core of 0.7 ms^{-1} in the upper 20 m and velocities of around 0.3 ms^{-1} down to 65 m depth. Alternating up- and downwelling velocities with values up to 10^{-3} ms^{-1} are seen extending from 10-m to 70-m depth. The front is also associated with strong vertical mixing, particularly on its cold side, with values as large as 0.016 m^2s^{-1}. Enhanced vertical mixing near the bottom may be associated with the coastal upwelling process, as SACW near the bottom is displaced shoreward during the upwelling season and not necessarily related to the frontal dynamics per se [39].

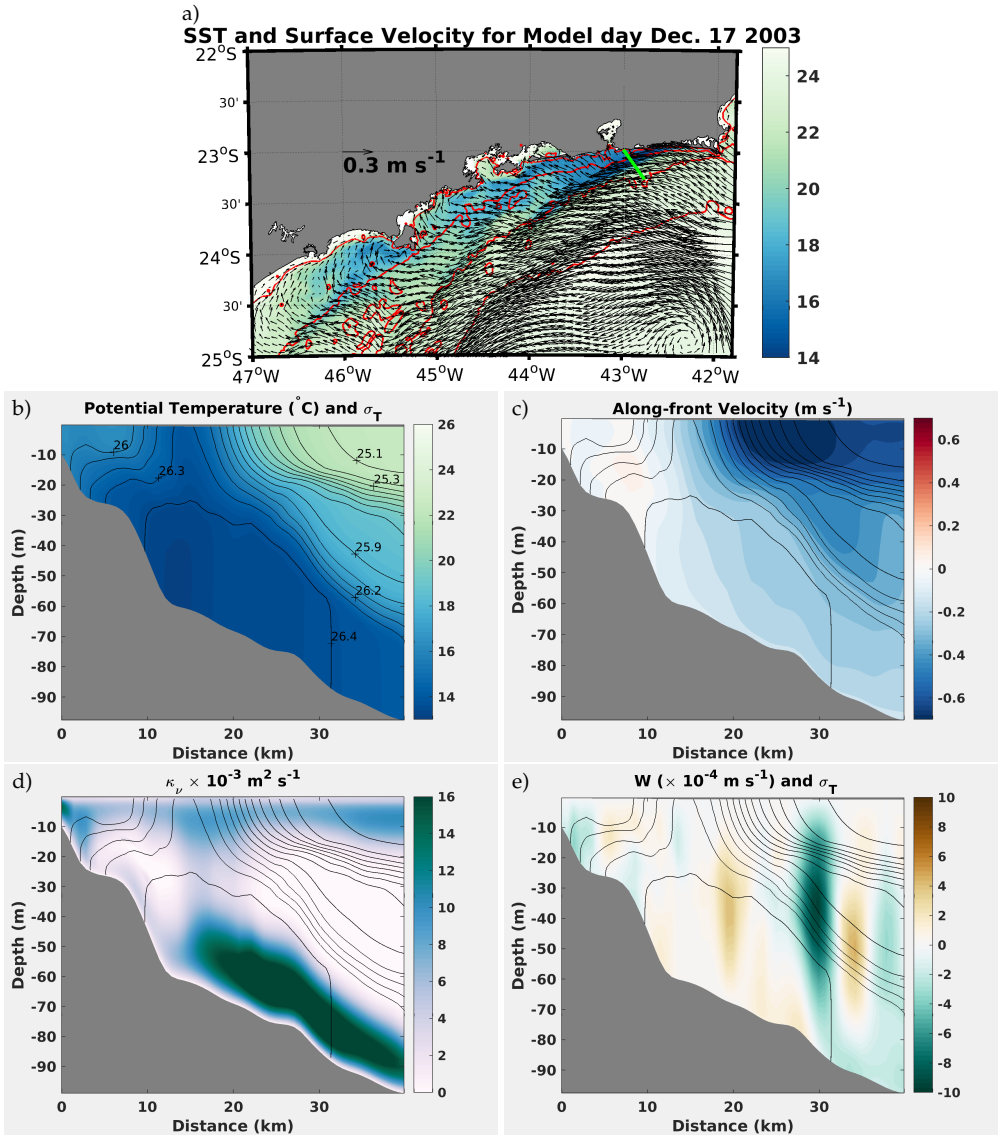

Figure 6. (**a**) Modeled SST (in °C) and surface velocities for 17 December 2003 with location of the transect highlighted in green. Red lines show the isobaths of 10 m, 50 m, 100 m, and 200 m. (**b**) Temperature transect across the front with associated isopycnals; (**c**) Along-front velocity transect; (**d**) Vertical viscosity coefficient transect; (**e**) Vertical velocity transect. All values are obtained from daily-averages of the model output. Isopycnals are shown in black.

Given the importance of vertical mixing within the front, the dynamical balance may be largely explained by the turbulent thermal wind (TTW) balance [36,37],

$$\overbrace{-f\frac{\partial v}{\partial z}}^{T1} = \overbrace{-\frac{\partial b}{\partial x}}^{T2} + \overbrace{\frac{\partial^2}{\partial z^2}\left(\kappa_v \frac{\partial u}{\partial z}\right)}^{T3} \tag{1a}$$

$$f\frac{\partial u}{\partial z} = -\frac{\partial b}{\partial y} + \frac{\partial^2}{\partial z^2}\left(\kappa_v \frac{\partial v}{\partial z}\right), \tag{1b}$$

where Equation (1a) refers to the along-front direction and Equation (1b) to the cross-front direction. $b = \frac{-g\rho}{\rho_0}$ is the buoyancy, where ρ is the density and ρ_0 is a reference density, in this case 1025 kgm^{-3}.

The dynamical balance calculated for the transect of Figure 6, using Equation (1), shows that although the TTW seems to be a good first-order approximation, as shown in Figure 7, it does not provide the full picture of the frontal dynamics. The unexplained part

of the balance may be due to tendency and advection as the front seems to be a consequence of both the coastal upwelling and horizontal advection due to intrusions of the BC onto the shelf. In order to investigate in more detail the dynamical balance of these features, we extract daily averages of each term of the momentum equation. The momentum equations in Cartesian coordinates are

$$\overbrace{\frac{\partial u}{\partial t}}^{Tendency} = \overbrace{-\vec{v_h}\cdot\nabla_h u}^{Horiz.Advection} \overbrace{-w\frac{\partial u}{\partial z}}^{Vert.Advection} \overbrace{+fv}^{Coriolis} \overbrace{-\frac{\partial \phi}{\partial x}}^{Pres.Gradient} \overbrace{+\frac{\partial}{\partial z}\left(\kappa_v \frac{\partial u}{\partial z}\right)}^{Vert.Mixing} \overbrace{+\mathscr{D}_u}^{Horiz.Mixing} \overbrace{+\mathscr{S}_u}^{Nudging} \quad (2a)$$

$$\frac{\partial v}{\partial t} = -\vec{v_h}\cdot\nabla_h v - w\frac{\partial v}{\partial z} - fu - \frac{\partial \phi}{\partial y} + \frac{\partial}{\partial z}\left(\kappa_v \frac{\partial v}{\partial z}\right) + \mathscr{D}_v + \mathscr{S}_v, \quad (2b)$$

where $\vec{v_h} = (u, v)$ is the horizontal velocity, $\nabla_h = (\frac{\partial}{\partial x}, \frac{\partial}{\partial y})$, ϕ is the dynamic pressure, $\mathscr{D}$ are diffusive terms, and $\mathscr{S}$ are nudging terms. The last two terms are negligible and are not shown. Figure 8 shows the remaining terms of Equation (2b) in the cross-frontal direction for the front shown in Figure 6. The vertical mixing term largely balances the sum of the pressure gradient and Coriolis terms in the upper 20 m. Part of this is due to the Ekman balance, in which wind-driven mixing balances the Coriolis force and is independent of the frontal structure. This is more common during the upwelling phase, when winds are stronger. Another part is due to mixing induced by the geostrophic flow within the front, which is associated with the TTW [37]. Between 20 km and 30 km, within the frontal jet, horizontal advection becomes important with a smaller contribution of vertical advection near 30 km.

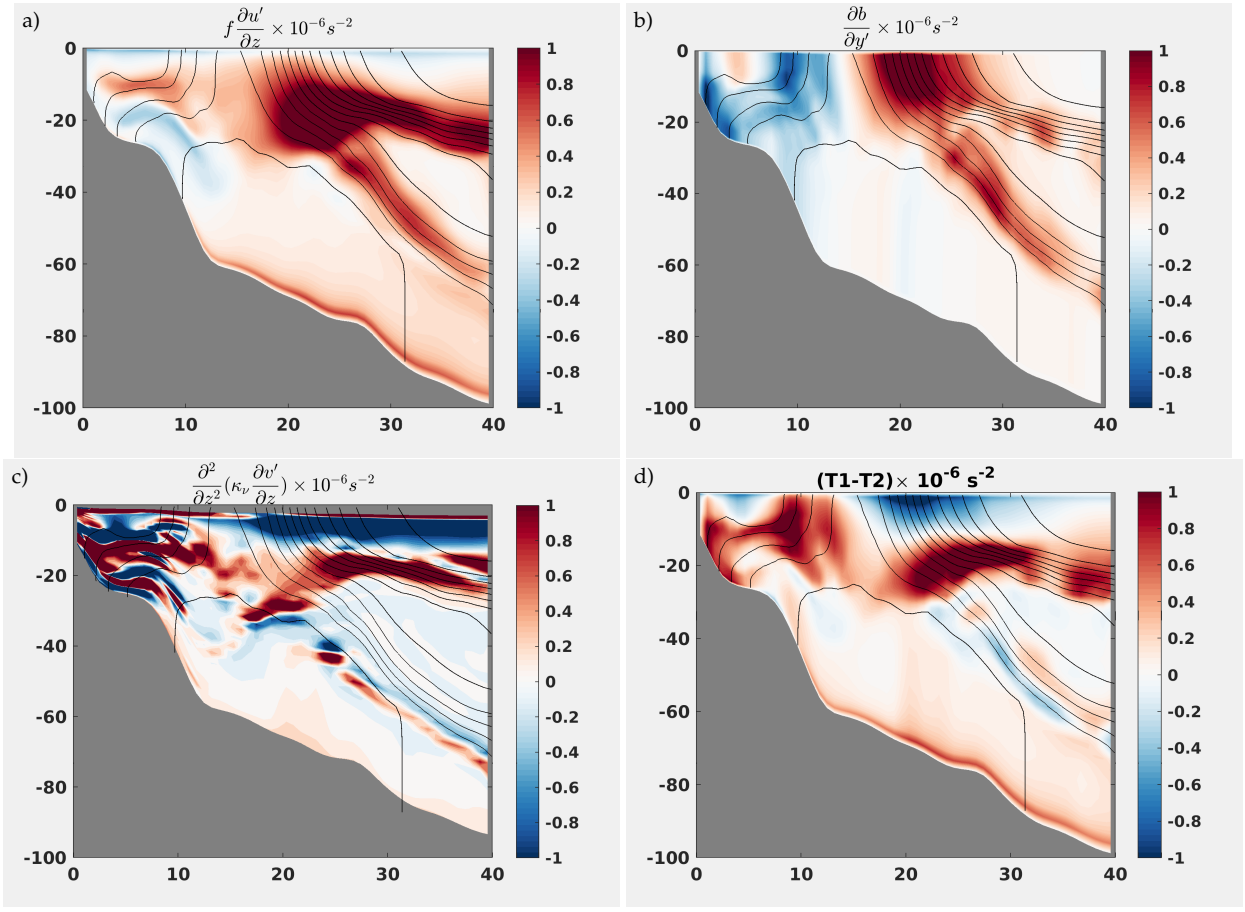

Figure 7. Terms from the turbulent thermal wind balance in the cross-frontal direction (Equation (1b)) calculated from the transect in Figure 6. (**a**) $f\frac{\partial u}{\partial z}$, (**b**) $\frac{\partial b}{\partial y}$, (**c**) $\frac{\partial^2}{\partial z^2}\left(\kappa_v \frac{\partial v}{\partial z}\right)$ and (**d**) the difference between terms shown in (**a**,**b**). Isopycnals are shown in black.

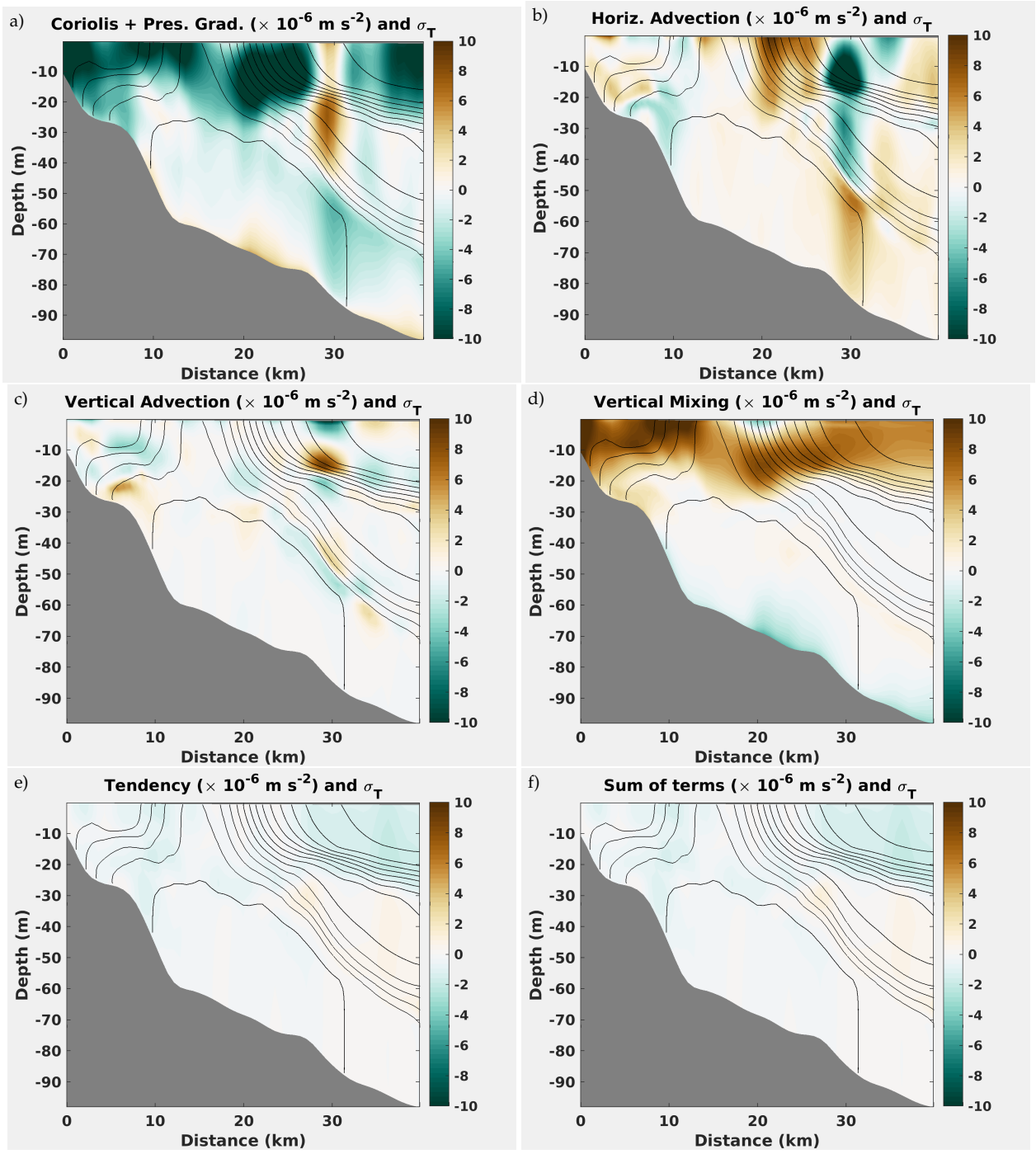

Figure 8. Terms from the meridional momentum equation in the cross-frontal direction calculated for the transect in Figure 6. Nudging and horizontal mixing terms are neglected.

3.2.2. Cold Filament

Cold filaments on the shelf are highly episodic, last no more than one or two days, and are characterized by large vertical mixing and convergence. They are common not only in the CF upwelling region but also in the wider continental shelf and the adjacent open ocean given the intermittent wind forcing and strongly sheared currents which can easily generate cold anomalies that are subsequently stretched and thinned. Figure 9 shows the evolution of one of the cold filaments modeled in the region in May, in the beginning

of the relaxation season. It is formed as a consequence of convergence and straining of the weakening upwelling center as it transitions from the upwelling to the relaxation season due to the subsiding winds and cooling. The whole process takes around 4 days and the cold filament itself reaches its strongest horizontal density gradient on 20 May. A vertical transect is taken on this day and is shown in Figure 10. The filament has a width of approximately 3 km and extends down to 20–30 m depth, roughly constrained within the surface mixed layer. Its most striking feature is the very large downwelling at its core, with vertical velocities as large as 1 cms^{-1}, consistent with previously modeled cold filaments [7,37]. This is caused by convergent velocities in the cross-filament direction in the upper 20 m (Figure 10). The cold filament is also associated with strong vertical mixing in the upper 20 m, as seen by the large values of the modeled κ_v.

Figure 11 shows each term from the TTW calculated from the transects shown in Figure 10. The vertical mixing term mostly balances the difference between the vertical shear of the along-front velocity and the cross-front buoyancy gradients. The TTW balance is not expected to be perfect, as it neglects the time tendency and advection terms, which are clearly important in this case. Nevertheless, the TTW provides a good estimate of the dynamical balance within the cold filament.

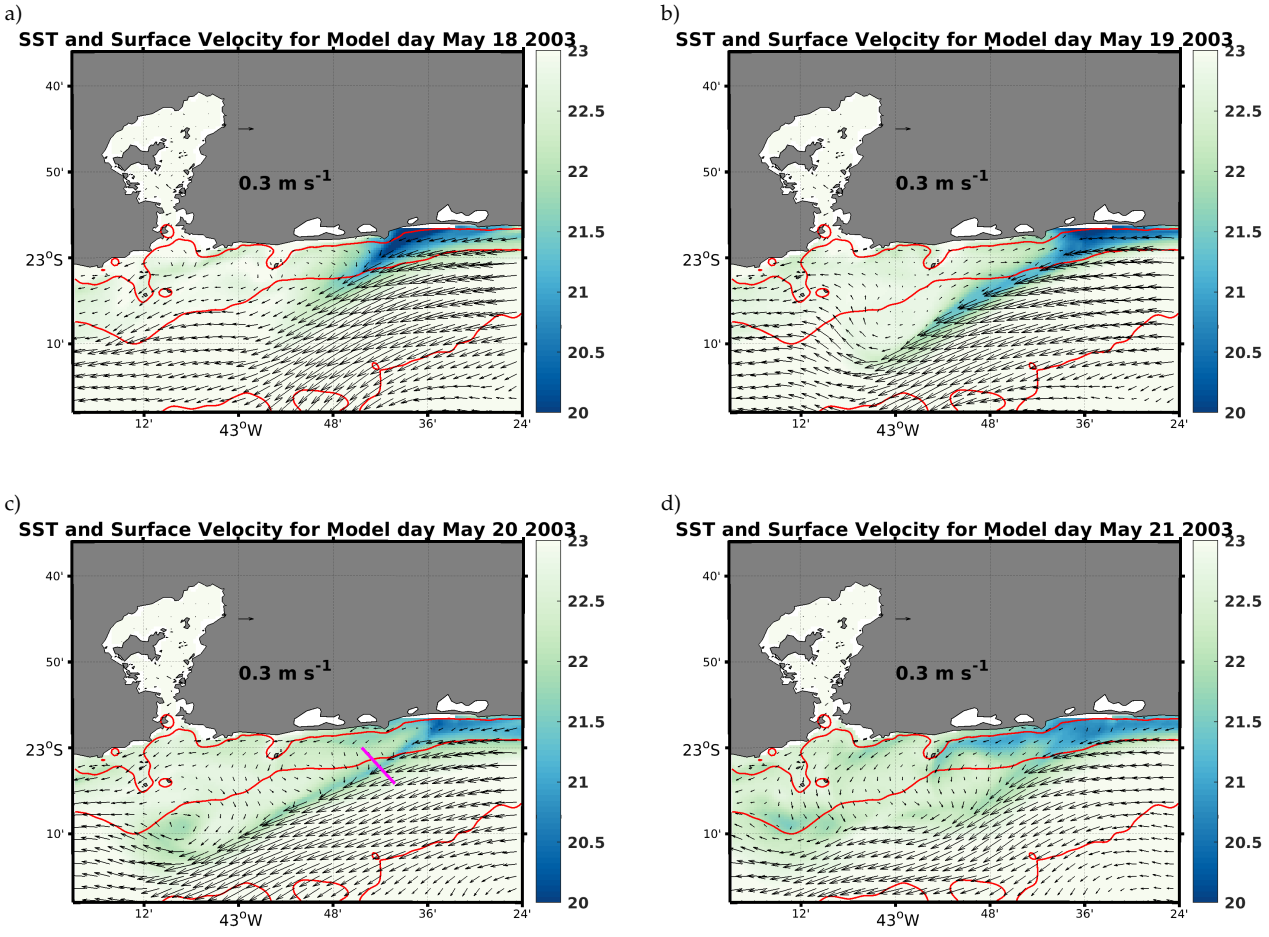

Figure 9. Modeled daily averages of SST (in °C) and surface velocities during the formation and dissipation of the cold filament. Dashed lines show the isobaths of 10 m, 50 m, and 100 m.

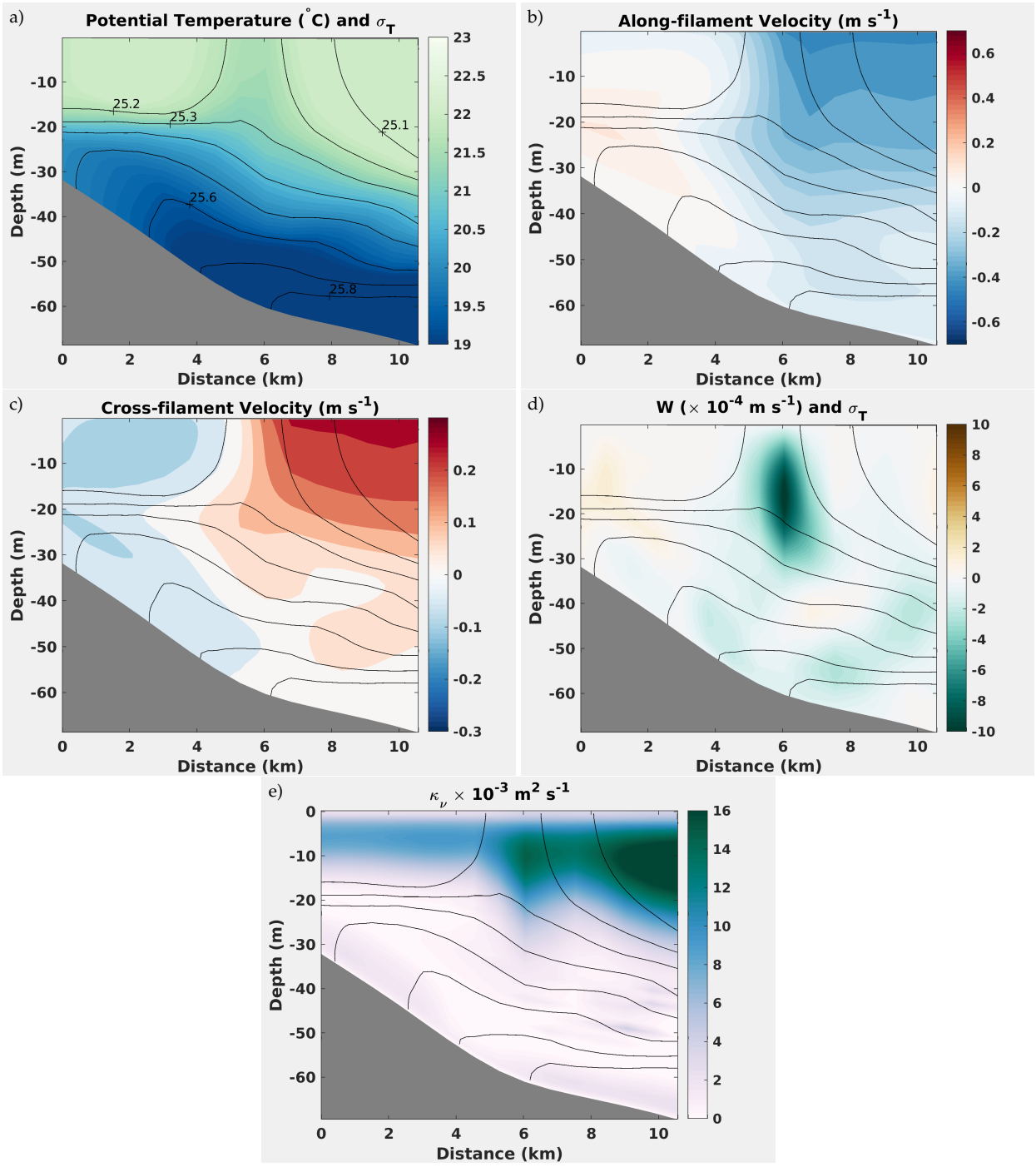

Figure 10. (**a**) Temperature transect across the filament shown in Figure 9c with associated isopycnals; (**c**) Along-filament velocity transect; (**c**) Cross-filament velocity transect; (**d**) Vertical velocity transect; (**e**) Vertical viscosity coefficient transect. All values are obtained from daily-averages of the model output. Isopycnals are shown in black.

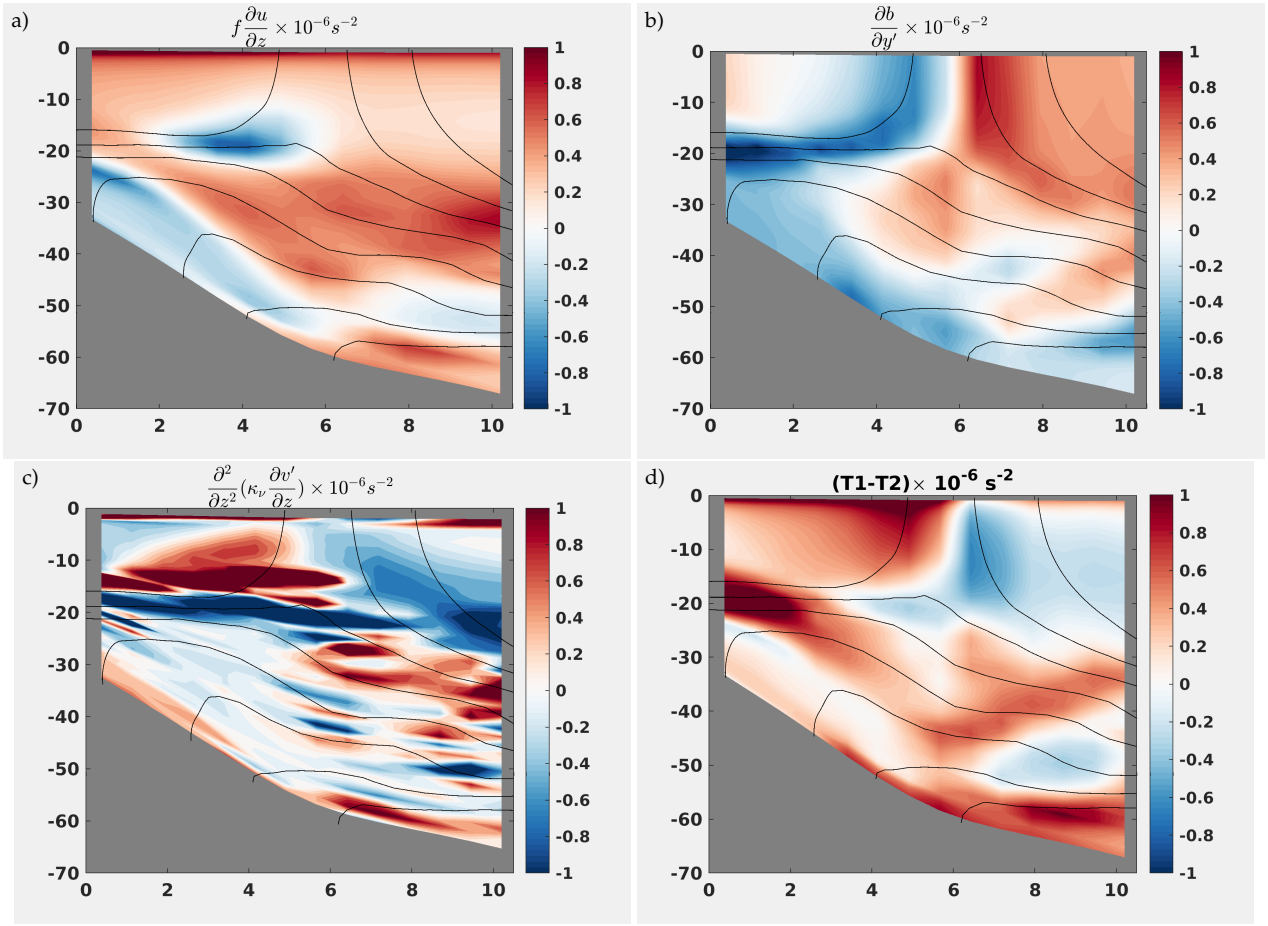

Figure 11. Terms from the turbulent thermal wind balance in the cross-filament direction (Equation (1b)) calculated from the transect in Figure 9c. (**a**) $f\frac{\partial u}{\partial z}$, (**b**) $\frac{\partial b}{\partial y}$, (**c**) $\frac{\partial^2}{\partial z^2}\left(\kappa_v \frac{\partial v}{\partial z}\right)$ and (**d**) the difference between terms shown in (**a**,**b**). Isopycnals are shown in black.

Analysis of each term of Equation (2b) in the cross-filament direction shows that departure from geostrophy is to a large extent balanced by vertical mixing which confirms that the TTW the dominant balance as seen from the alternating pattern of the vertical mixing term on the different sides of the filament (Figure 12). Horizontal and vertical advection are also important terms, which is to be expected because the filament deviates from the prototype TTW which applies for fronts or filaments that are nearly straight, have little ageostrophic secondary circulation, and are in steady state.

3.2.3. Coastal Coherent Eddy

A clearer distinction in terms of coherent structures formed in the coastal and shelf region of the SBB can be seen in the relaxation phase, from April to September. Weaker winds cause a reduction or cessation of the coastal upwelling and coastal downwelling in some occasions. Surface cooling also tends to homogenize the upper 50 m of the water column near the coast, as opposed to a mostly two-layered system with TW on top of SACW during the upwelling season. These conditions, associated with horizontal shear at CF, where the coastline abruptly changes direction, favor the formation of coherent cyclonic eddies which can propagate on the shelf for several months. The predominance of cyclonic vorticity at this location is evident in mean, variance, and the positive skewness of relative vorticity (Figure 5). The values are consistently positive starting from CF and following roughly the 100 m isobath.

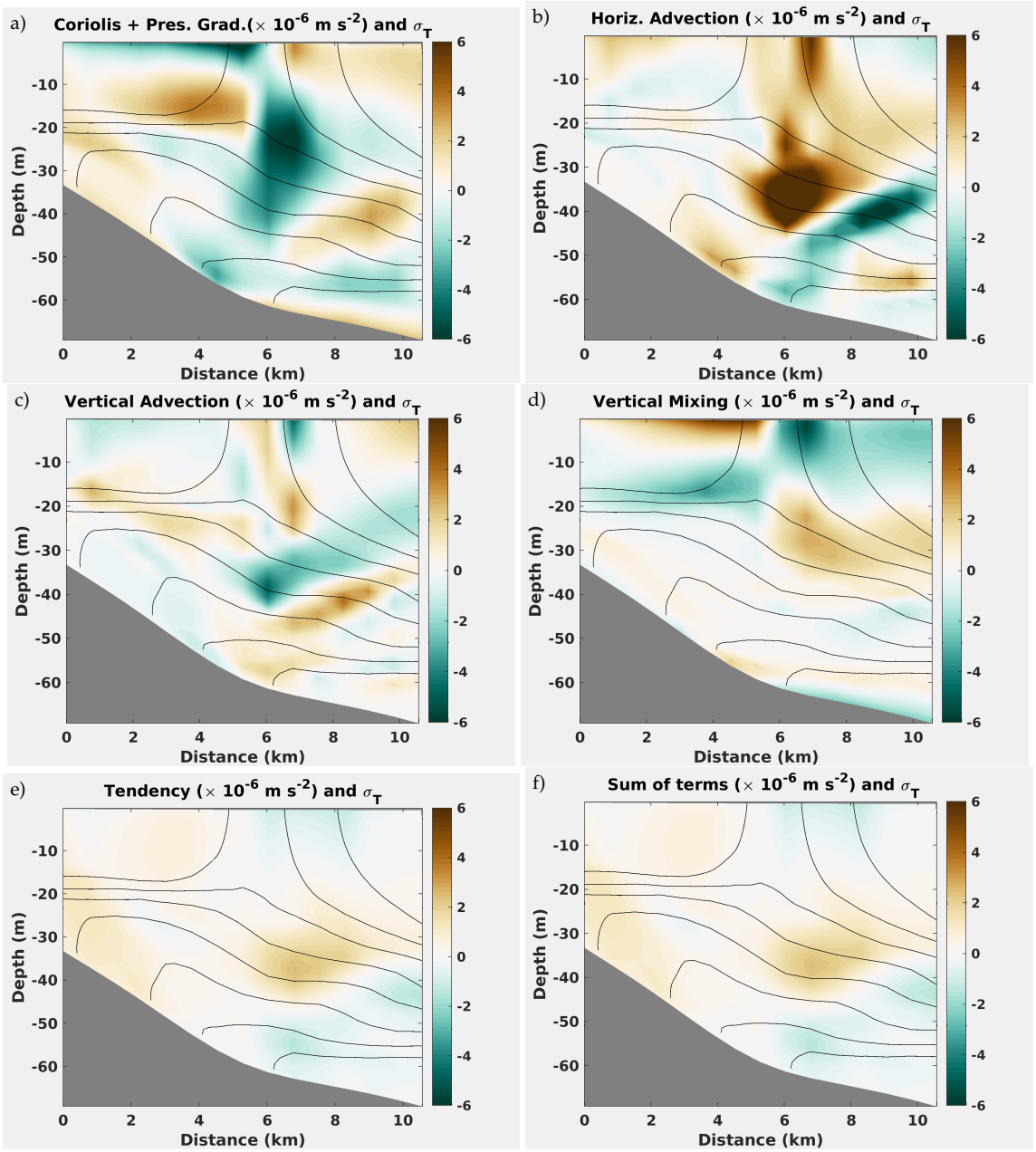

Figure 12. Terms from the meridional momentum equation in the cross-filament direction calculated for the transect in Figure 9c. Nudging and horizontal mixing terms are neglected.

These vortices are different in size, relative vorticity, and formation mechanisms from the well known cyclonic eddies associated with instabilities of the Brazil Current system [40]. Because the Rossby radius of deformation on the shelf is, approximately, 10 km, these coastal eddies, whose diameter is around 20 km, should be characterized as mesoscale. From a dynamical point of view, this is an important distinction and shows the need to look at the different processes observed on the shelf not only in terms of their nominal length scales but also in terms of how they compare to other dynamically relevant quantities, such as the deformation radius.

Figure 13 shows one of the modeled eddies right after its formation, on 23 May 2003 and six days later when it is a coherent feature detached from the coast. Note the similarity in terms of size and location with the eddy detected in the SST image shown in Figure 4 at approximately the same date. Figure 14 shows that the vertical structure of the eddy on 29 May 2003 is mostly confined to the upper layer. Vertical mixing within the eddy is much

smaller than in its surroundings, where large values are associated with cooling. Very large vertical velocities are seen in narrow regions within and on the flanks of the eddy.

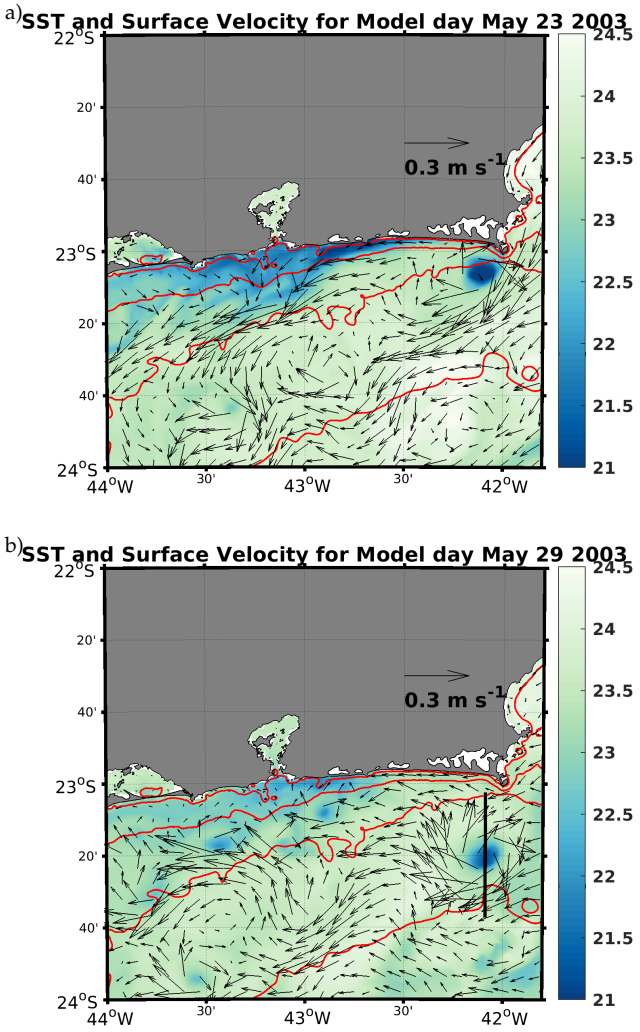

Figure 13. Modeled daily averages of SST (in °C) and surface velocities during the formation of a coastal eddy and its separation from the coast 6 days later. Red lines show the isobaths of 10 m, 50 m, 100 m, and 200 m.

The terms in Equation (1) are calculated for the meridional transect shown in Figure 13b and show that it is largely in gradient-wind balance (Figure 15), as the difference between the vertical shear and the buoyancy gradient terms suggests that the centrifugal force may be important. A back of the envelope calculation shows that $\frac{V^2}{R}$ equals 3.60×10^{-5} ms^{-2} using a maximum velocity of 0.6 ms^{-1} and the radius of the eddy of 10 km. This is roughly the same value as fV, which is 3.42×10^{-5} ms^{-2}, using $f = -5.8 \times 10^{-5}$ s^{-1}. Therefore, the centrifugal force can not be neglected.

The analysis of the momentum budget in the meridional direction (Figure 16) confirms that Coriolis, pressure gradient, and horizontal advection are the largest terms within the eddy, with a small but non-negligible contribution of vertical advection. No strong surface mixing is associated with the eddy, as opposed to the filament and the front discussed above. These eddies can, however, have a significant impact on the shelf circulation as they carry coastal waters into the mid- and outer shelf. Their lifetimes range from a few days to many months. In this specific example, the eddy propagates southwestward as a coherent feature for 4 months, decaying on model day 22 August 2003 at 46.90° W, 25.43° S.

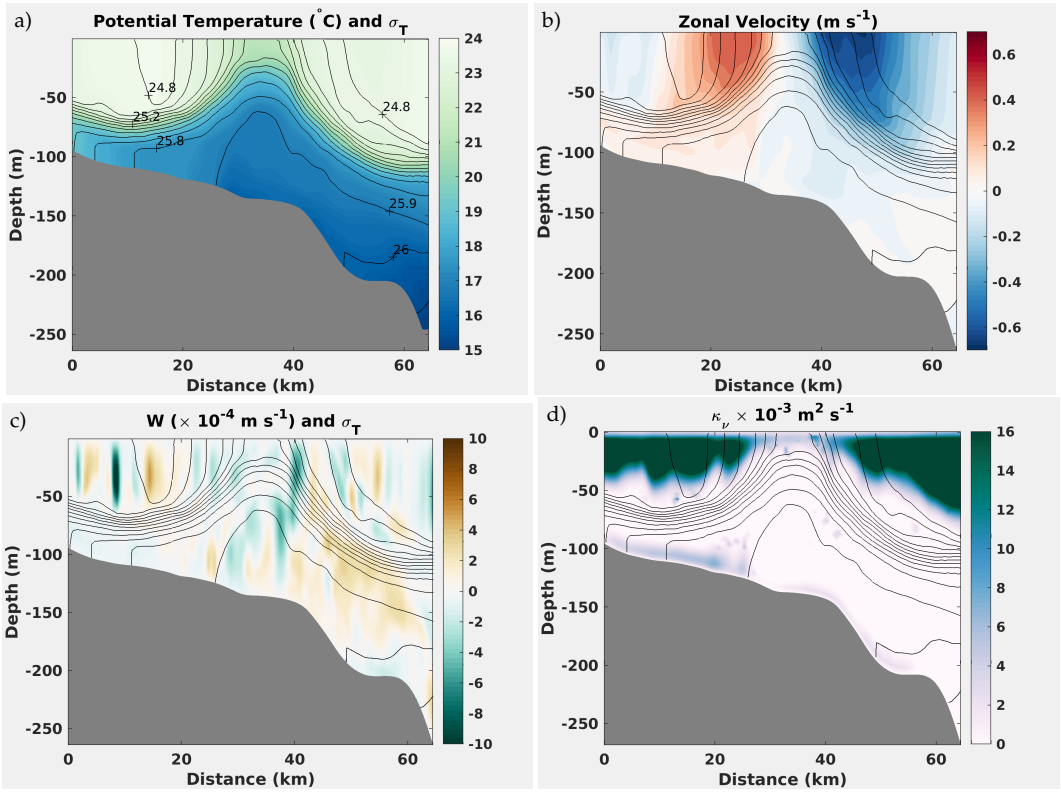

Figure 14. (**a**) Temperature transect across the coastal shown in Figure 13b with associated isopycnals; (**b**) zonal velocity transect; (**c**) Vertical velocity transect; (**d**) Vertical viscosity coefficient transect. All values are obtained from daily-averages of the model output. Isopycnals are shown in black.

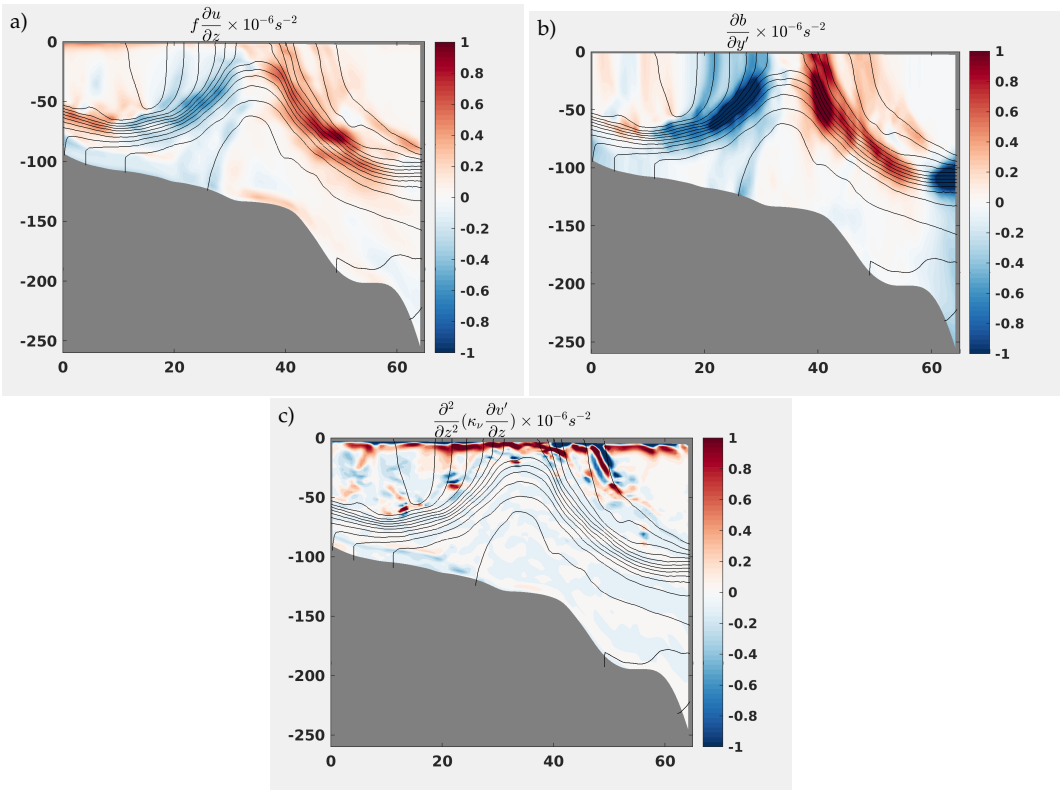

Figure 15. Terms from the turbulent thermal wind balance in the meridional direction across the coastal eddy (Equation (1b)) calculated from the transect in Figure 13b. (**a**) $f\frac{\partial u}{\partial z}$, (**b**) $\frac{\partial b}{\partial y}$, (**c**) $\frac{\partial^2}{\partial z^2}\left(\kappa_\nu \frac{\partial v}{\partial z}\right)$. Isopycnals are shown in black.

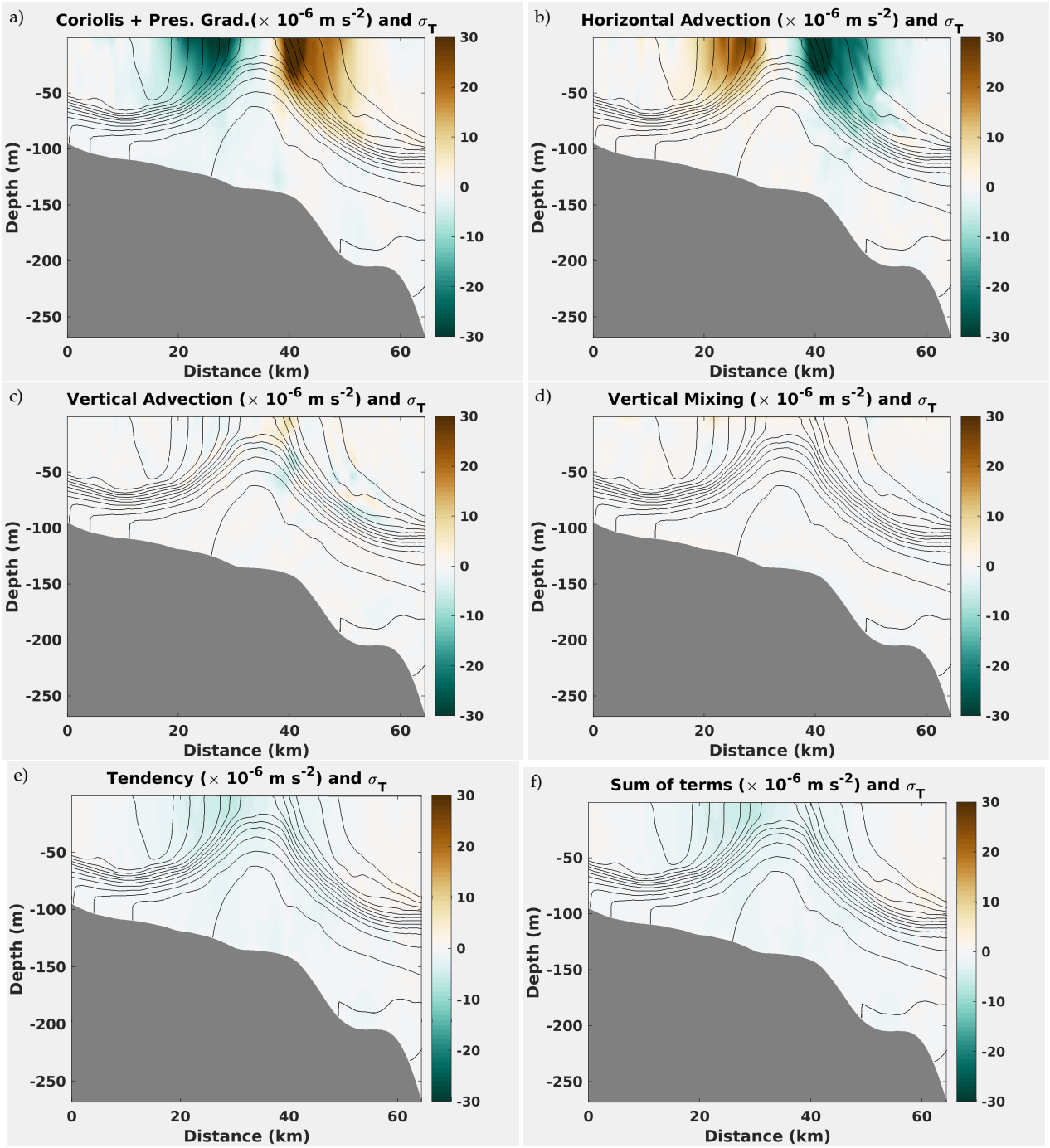

Figure 16. Terms from the meridional momentum equation calculated for the transect in Figure 9c. Nudging and horizontal mixing terms are neglected.

3.3. Energy Analysis

The eddy kinetic energy (EKE) was calculated for the Cape Frio upwelling region (the green rectangle in Figure A1) and averaged in the upper 50 m of the water column (Figure 17). We define the daily-averaged output as the total field, $\vec{v} = \overline{\vec{v}} + \vec{v'}$, where $\overline{\vec{v}}$ is the monthly average and $\vec{v}'$ are deviations from the average. The time-series of the averaged EKE shows that it is larger during periods when the upwelling front is not as intense. Note the peak from days 100 to 160, which is the period when the filament and the eddy previously analyzed occurred. This suggests that a strong front would hinder the local formation of eddies. This does not mean that the front is stable but rather that

the instabilities generated at the front may be horizontally advected and develop further downstream, while during the relaxation phase coherent eddies are formed locally.

In order to gain insight into the energy sources responsible for the features analyzed previously, we calculate the energy conversion terms in the coastal upwelling region and compare them with similar terms in the adjacent open ocean. The conversion from mean to eddy kinetic energy, the total shear production (SP), may be divided into a sum of the horizontal shear production (HSP) and the vertical shear production (VSP) [41,42]

$$SP = HSP + VSP, \tag{3}$$

where

$$HSP = -\overline{u'^2}\frac{\partial \overline{u}}{\partial x} - \overline{u'v'}\frac{\partial \overline{u}}{\partial y} - \overline{v'^2}\frac{\partial \overline{v}}{\partial y} - \overline{u'v'}\frac{\partial \overline{v}}{\partial x}, \tag{4a}$$

$$VSP = -\overline{u'w'}\frac{\partial \overline{u}}{\partial z} - \overline{v'w'}\frac{\partial \overline{v}}{\partial z}, \tag{4b}$$

$$BP = \overline{w'b'}. \tag{4c}$$

The analysis allows one to infer the preponderance of baroclinic instability, if BP > 0, barotropic instability, if HSP > 0, or vertical shear instability, if VSP > 0.

We calculated these terms for an area representative for the coastal upwelling center (the green box in Figure A1) and box-averaged them in the upper 50 m, based on the vertical extent of the previously analyzed structures. Figure 18a shows the evolution of each averaged term over the whole year of simulation. In the first 100 days, roughly from January to the beginning of April (the upwelling phase), baroclinic and barotropic instabilities are dominant. The relatively high-frequency (≈7 days) oscillations are due to coastal currents driven by the local winds and by the passage of continental shelf waves that flow along the coast as seen from variations on sea surface height (see Figure 3(middle)). Upwelling-favorable winds bring colder water to the surface which can lead to large horizontal buoyancy gradients, a strong thermal-wind jet, and baroclinic instability. Coastal intrusions of the BC onto the shelf at CF may also enhance the jet and lead to large horizontal shear production. During mid-April until the end of June (the relaxation phase) baroclinic instability dominates. This is the period when coherent, cyclonic eddies are preferentially formed in the region. Buoyancy production is larger during the period when stratification in the upper 50 m is weaker because during the upwelling phase the stratification induced by coastal upwelling and the intrusion of SACW is included in the the mean. Therefore, the anomalies, and hence BP, are smaller. During the relaxation phase, sporadic events generate anomalies at the coast which are not horizontally advected because of the absence of the front and weaker currents. This allows instabilities to grow locally. As an illustration, we show the evolution of modeled SST and surface velocities after a strong burst of upwelling-favorable winds on 7 September (day 250 in Figure 3(top)). Note that the SST is not as cold as during the upwelling phase, but the deviation from the mean is significant. In 4 days, from 7 September to 11 September, colder waters emerge in the CF upwelling center, but a reversal of the winds induces an increase in sea level and a coastal current flows eastward, giving rise to strong horizontal shear which result in five cyclonic eddies along the 100-m isobath on 17 September (Figure 19), the same location of large cyclonic vorticity skewness as shown in Figure 5.

In the remainder of the year, a mixed barotropic-baroclinic instability pattern is predominant. Note the positive bias in both BP and HSP which suggests that, on average, there is a supply of energy from the mean to the eddy flow in the region from both the horizontal shear and the eddy buoyancy flux. As a comparison, Figure 18b shows the same calculation for an area on the adjacent open ocean (the green rectangle in Figure A1) where a very different pattern is observed, with episodic—but at lower frequency than in the coastal case—bursts of HRS due to the mesoscale eddies formed by instabilities of the BC and increased eddy buoyancy flux from early autumn to late winter. Note that

PeKe in this case may be underestimated as the buoyancy anomalies within open-ocean, mesoscale eddies will reach deeper than 50-m. In the open ocean case, however, only the eddy buoyancy flux has a positive average over the year, showing that baroclinic instability, on average, is the dominant process for eddy variability. The large positive and negative values of HRS tend to average out over the year.

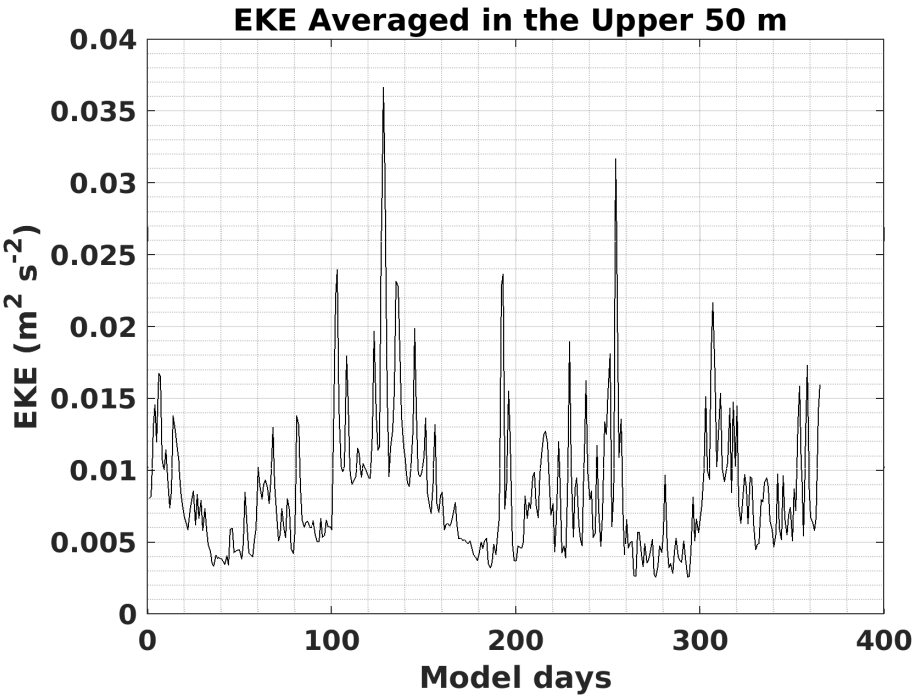

Figure 17. Box-averaged eddy kinetic energy in the upper 50 m of the water column over the Cape Frio upwelling region.

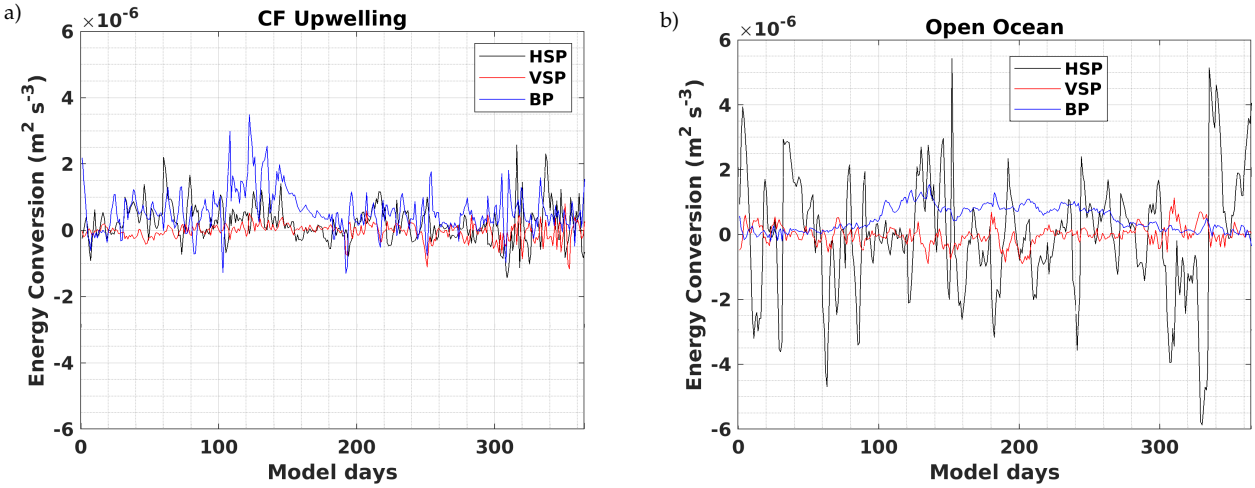

Figure 18. Time-series of the terms shown in Equation (4) for (**a**) the CF upwelling region and (**b**) the adjacent open ocean. All terms are calculated within the rectangles shown in Figure A1 and averaged in the upper 50 m.

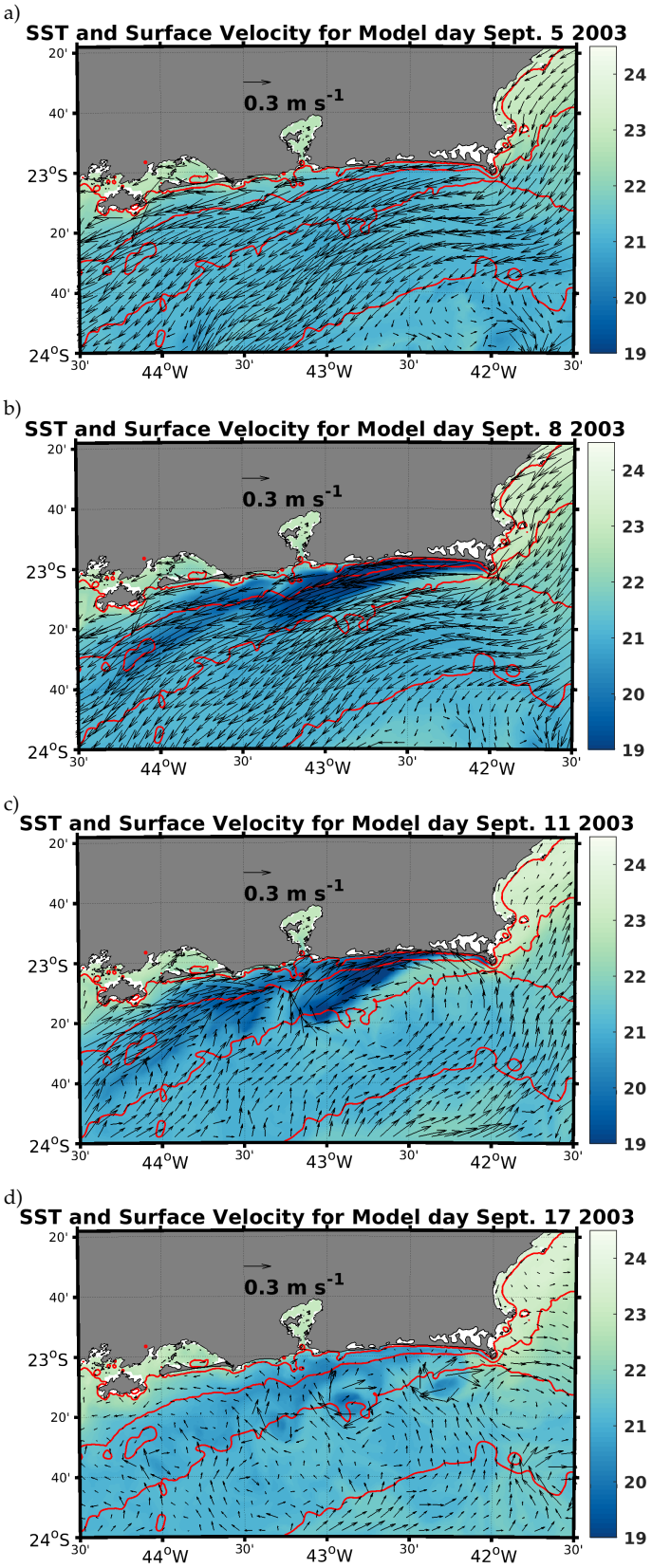

Figure 19. Modeled daily averages of SST (in °C) and surface velocities after a strong wind event on 7 September (day 250) which causes coastal upwelling and the subsequent formation of shear-induced, coastal cyclonic eddies. Dashed lines show the isobaths of 10 m, 50 m, 100 m, and 200 m.

4. Discussion and Conclusions

Our model simulation shows that during the upwelling phase, roughly from late October to late March, the dominant feature is an upwelling front east of Cabo Frio. It is an elongated stretch around 200 km long and 20 km wide with horizontal temperature gradients as large as 8 °C over less than 10 km . The front is characterized by a strong jet and is associated with enhanced vertical mixing. The dynamical balance within the front may be described as a sum of Ekman and turbulent thermal wind. The large horizontal velocities transport cold and nutrient-rich water hundreds of kilometers away from the CF upwelling region [24]. This preferential route of cross-shelf export of coastal, nutrient-rich, recently upwelled waters can be very important for larval transport and fisheries [43] as well as benthic production [44,45] in the region. The existence of a strong front may hinder the formation of coherent eddies locally. This is consistent with theoretical studies showing that frontal regions associated with strong stretching inhibit the amplification of disturbances that lead to the formation of coherent eddies [46,47]. It may also be that the instabilities generated in the front are strongly advected and their effect is seen downstream, which is what is seen in the model results to a certain extent. However, this meandering when the front is strong does not lead to the formation of coherent eddies.

During the relaxation phase, from late April to late September, winds subside, the frontal jet weakens and the water column becomes less stratified in the upper 50 m. In this period, our model simulation shows a preference for the formation of coherent cyclonic eddies. They carry coastal waters across the continental shelf and could be an important cross-shelf transport mechanism of water properties and organisms that make use of these structure to maintain a high level of spawning activity even during the winter, such as the *Engraulis anchoita* [43]. The fact that these eddies maintain their coherency for many months could be very useful for different species as a sheltered environment that would favor the survival of larvae that would perish otherwise.

Because the horizontal scale of eddies (≈20 km) is comparable to the shelf radius of deformation (≈10 km), these features should be characterized as mesoscale. This is corroborated by the fact that these eddies are mostly in gradient-wind balance. Nevertheless, they are one order of magnitude smaller than the open ocean mesoscale eddies and associated with small patches of very large vertical velocities on their flanks, so they are prone to the development of submesoscale motions.

An analysis of the energy conversion terms show that during the upwelling phase horizontal shear production and buoyancy production dominate, suggesting a mixture of baroclinic and barotropic instabilities in the upwelling center. During the relaxation phase, baroclinic instability dominates. Note that there is significant time-variability associated with these terms, which could be associated with the wind forcing, continental shelf waves, and relaxation events on shorter time-scales. Our results corroborate recent work showing that baroclinic instability maintains a strong mesoscale eddy field on the shelf on scales comparable to the shelf deformation radius [48,49].

The straining of the surface, cold temperature anomalies, and horizontal convergence gives rise to the third feature highlighted in this work, namely, cold filaments. They are ephemeral and last no more than one or two days. In our model simulation, the width of the cold filaments is around 1 km; therefore, even our 500-m simulation is not sufficient for a full description of their dynamics. Downwelling velocities as large as 1 cms^{-1} and strong vertical mixing is observed in their center. The turbulent thermal wind is shown to be the leading order balance within the analyzed feature. There was no clear seasonality associated with these features as episodic coastal upwelling events, surface convergence, and horizontal straining are present throughout the year. The large downwelling in relatively shallow regions makes the cold filaments potentially important for sediment transport and the export of coastal organic material from the surface to the bottom of the ocean, thus being important for the productivity of benthic organisms [44,45].

Given the importance of the CF upwelling region on the productivity of the SBB, both locally and remotely, and the ubiquity of fronts, eddies and filaments on the shelf, it is

important to take these features into account for a better understanding of the functioning of this ecosystem and its resilience to direct human activities (e.g., oil exploration, fisheries, tourism) and to climate change.

Author Contributions: Conceptualization, P.H.R.C.; methodology, P.H.R.C., N.S.; software, P.H.R.C.; validation, P.H.R.C.; formal analysis, P.H.R.C., N.S.; investigation, P.H.R.C., N.S., B.B., I.C.A.d.S.; resources, P.H.R.C.; data curation, P.H.R.C.; writing—original draft preparation, P.H.R.C., N.S.; writing—review and editing, P.H.R.C., N.S., B.B., I.C.A.d.S.; visualization, P.H.R.C.; supervision, P.H.R.C.; project administration, P.H.R.C.; funding acquisition, P.H.R.C., B.B. All authors have read and agreed to the published version of the manuscript.

Funding: This work was supported by the PACES-II Program (Polar Regions and Coasts in the changing Earth System) of the Helmholtz Association.

Acknowledgments: The model simulations were performed on the HPC cluster *Strand* at the Helmholtz-Zentrum Geesthact. We thank the cluster team for the maintenance of the system.

Conflicts of Interest: The authors declare no conflict of interest. The funders had no role in the design of the study; in the collection, analyses, or interpretation of data; in the writing of the manuscript, or in the decision to publish the results.

Appendix A. Model Validation

Appendix A.1. The Brazil Current System

In this section we show some annually- and seasonally-averaged properties obtained from one year of our model simulations in order to provide a degree of dynamical consistency for our results. It is important to show that the large- and mesoscale fields are consistent with observational estimates. A one-year average is not adequate as a long-term average as specific mesoscale features may be too pronounced and influence the mean field. Nevertheless, our model does show the main features of the western South Atlantic, namely the BC and its meanders and eddies near Cabo Frio (Figure A1).

The annual average of the velocity along and across the transect from Figure A1 is shown in Figure A2, where we see the vertical structure of the Brazil Current system as currently understood at this location, namely the surface intensified BC flowing southward along the shelfbreak and the Intermediate Western Boundary Current (IWBC) flowing northward deeper at the slope. The BC-IWBC system is studied in detail in [25,27]. The annual average of the BC transport is 2.9Sv and for the IWBC it is 2.2Sv. Figure A3 shows a TS-diagram for the transect during the summer and winter months, showing that the vertical structure of water masses is consistent with the current knowledge of the region.

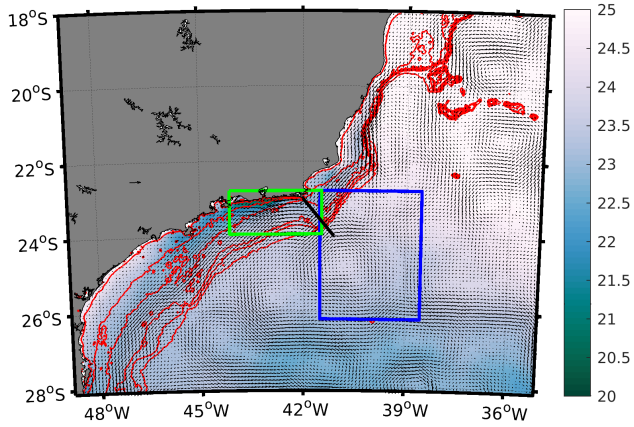

Figure A1. Annual average of the modeled SST in °C (color) and velocity (arrows). Squares show the region where the energy analysis in Section 3.3 was performed for the upwelling center and offshore. The black line shows the transect along which the average velocity was calculated.

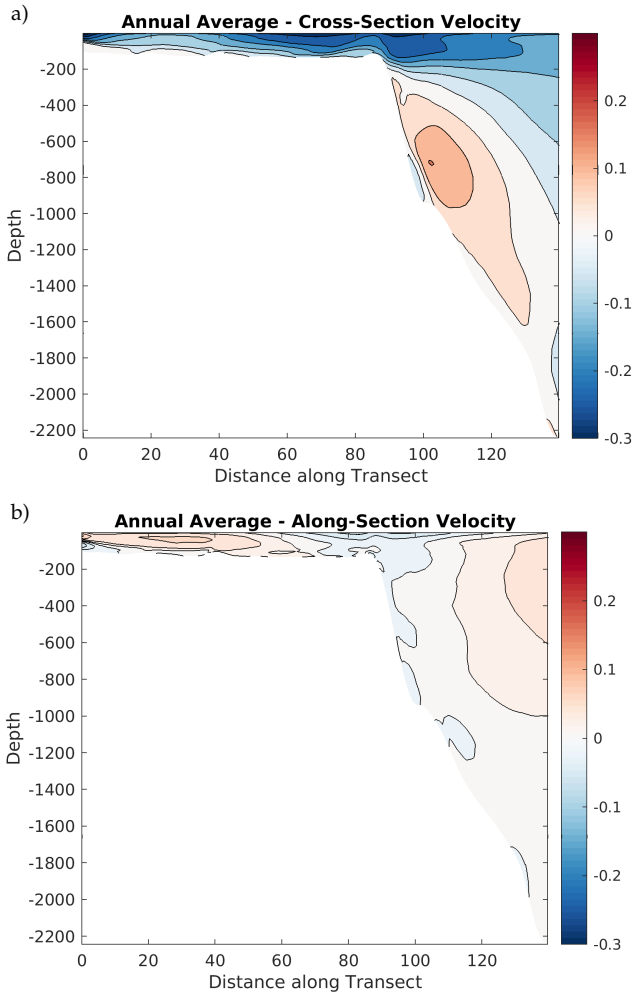

Figure A2. Annual average of the velocity along the transect shown in black in Figure A1. The structure of the western boundary current system of the South Atlantic ocean is consistent with observed estimates as shown by the southward-flowing Brazil Current in the upper 150 m and the northward-flowing Intermediate Western Boundary Current below.

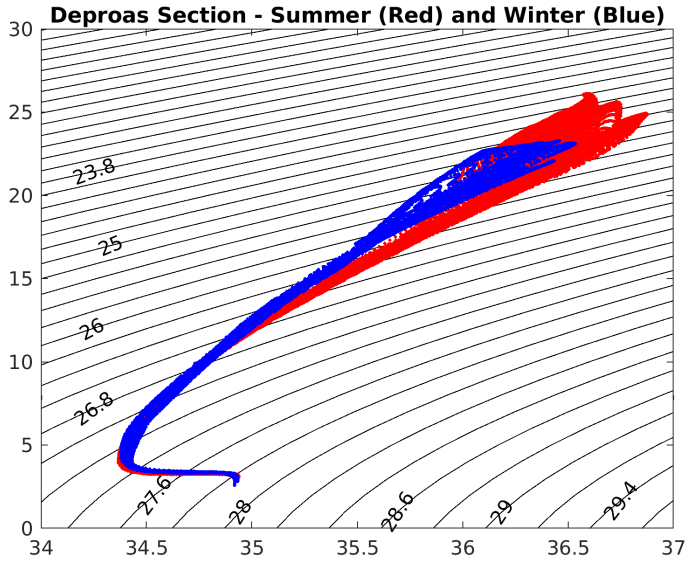

Figure A3. Temperature-Salinity diagram for the section shown in Figure A2 for the summer and winter months.

Appendix A.2. Distribution of Water Masses in the Northern SBB

In this section, we look at the distribution of temperature and salinity properties in the northern section of the SBB. The main deficiency of the model is that it does not contain the low salinity values that are important for the stratification of the inner shelf [28]. This is expected as we do not prescribe river flows in the current simulation. This is, however, not a serious drawback for the current study as we focus on the mid- and outer shelf dynamics. Other than that, both the structure of the temperature and salinity on the northern SBB during summer and winter at different depths (Figures A4 and A5) are consistent with the climatological estimates of [23], which is the most comprehensive dataset for the region to date. Specifically, we note the minima in temperature and salinity south of CF where bottom intrusions of SACW occur due the influence of mesoscale eddies [50] or topographic steering of the Brazil Current onto the coast [51]. In addition, the TS-diagrams (Figure A6) for the northern SBB are consistent with the observations except for the low salinity values on the inner shelf, as previously mentioned.

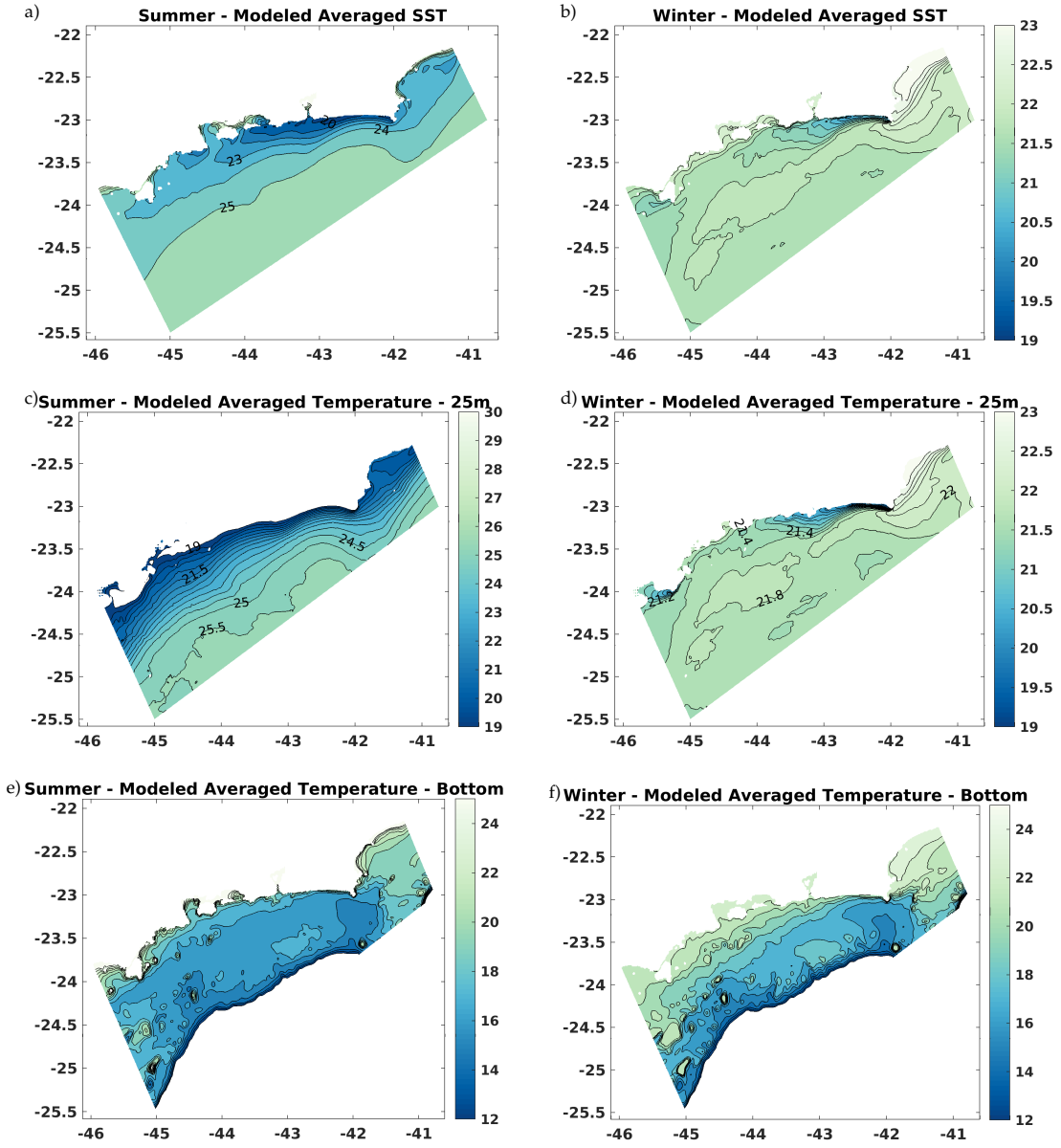

Figure A4. Summer (Jan-Mar) and winter (July-September) averages for temperature on the northern South Brazil bight at the surface, 25 m and the bottom).

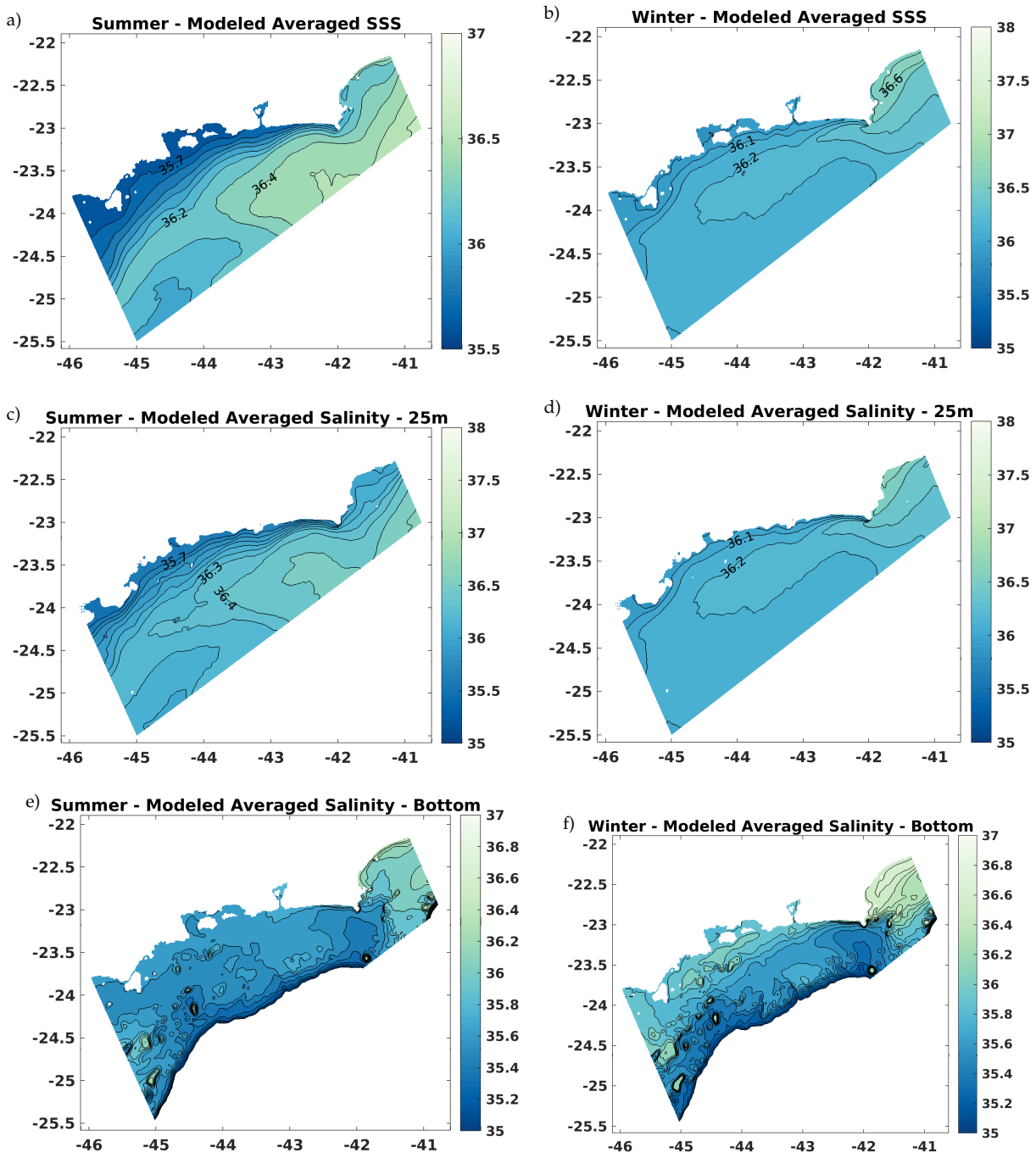

Figure A5. Summer (Jan-Mar) and winter (July-September) averages for salinity on the northern South Brazil bight at the surface, 25 m and the bottom.

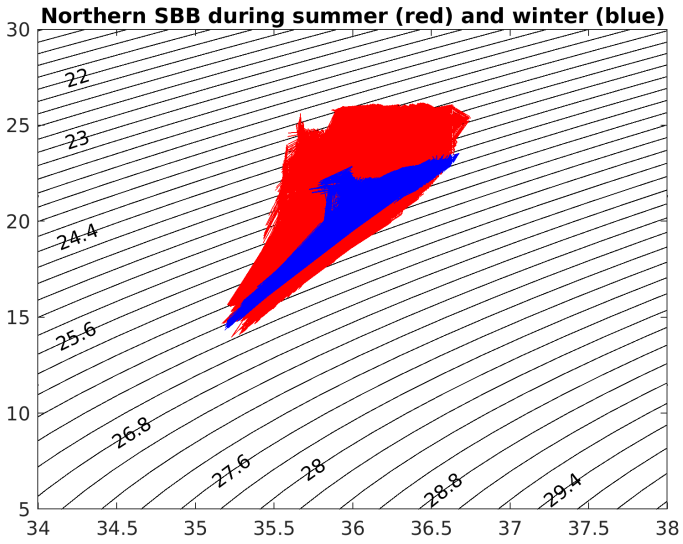

Figure A6. Temperature-Salinity diagram for the section shown in Figure A4 for the summer and winter months.

References

1. Flament, P.; Armi, L. The Shear, Convergence, and Thermohaline Structure of a Front. *J. Phys. Oceanogr.* **2000**, *30*, 51–66. [CrossRef]
2. Flament, P.; Armi, L.; Washburn, L. The evolving structure of an upwelling filament. *J. Geophys. Res.* **1985**, *90*, 11765. [CrossRef]
3. García-Muñoz, M.; Arístegui, J.; Pelegrí, J.L.; Antoranz, A.; Ojeda, A.; Torres, M. Exchange of carbon by an upwelling filament off Cape Ghir (NW Africa). *J. Mar. Syst.* **2005**, *54*, 83–95. [CrossRef]
4. Bassin, C.J.; Washburn, L.; Brzezinski, M.; McPhee-Shaw, E. Sub-mesoscale coastal eddies observed by high frequency radar: A new mechanism for delivering nutrients to kelp forests in the Southern California Bight. *Geophys. Res. Lett.* **2005**, *32*. [CrossRef]
5. Capet, X.; McWilliams, J.C.; Molemaker, M.J.; Shchepetkin, A.F. Mesoscale to Submesoscale Transition in the California Current System. Part I: Flow Structure, Eddy Flux, and Observational Tests. *J. Phys. Oceanogr.* **2008**, *38*, 29–43. [CrossRef]
6. Thomas, L.N.; Tandon, A.; Mahadevan, A. Submesoscale processes and dynamics. In *Ocean Modeling in an Eddying Regime*; Hecht, M.W., Hasumi, H., Eds.; American Geophysical Union: Washington, DC, USA, 2008; pp. 17–38. [CrossRef]
7. McWilliams, J.; Colas, F.; Molemaker, M. Cold filamentary intensification and oceanic surface convergence lines. *Geophys. Res. Lett.* **2009**, *36*, L18602. [CrossRef]
8. García-Muñoz, M.; Arístegui, J.; Montero, M.F.; Barton, E.D. Distribution and transport of organic matter along a filament-eddy system in the Canaries – NW Africa coastal transition zone region. *Prog. Oceanogr.* **2004**, *62*, 115–129. [CrossRef]
9. Schubert, R.; Schwarzkopf, F.U.; Baschek, B.; Biastoch, A. Submesoscale Impacts on Mesoscale Agulhas Dynamics. *J. Adv. Model. Earth Syst.* **2019**, *11*, 2745–2767. [CrossRef]
10. Fox-Kemper, B.; Ferrari, R. Parameterization of Mixed Layer Eddies. Part II: Prognosis and Impact. *J. Phys. Oceanogr.* **2008**, *38*, 1166–1179. [CrossRef]
11. Soh, H.S.; Kim, S.Y. Diagnostic Characteristics of Submesoscale Coastal Surface Currents. *J. Geophys. Res. Ocean.* **2018**, *123*, 1838–1859. [CrossRef]
12. Kirincich, A. The occurrence, drivers, and implications of submesoscale eddies on the Martha?s Vineyard inner shelf. *J. Phys. Oceanogr.* **2016**, *46*, 2645–2662. [CrossRef]
13. Marmorino, G.O.; Smith, G.B.; North, R.P.; Baschek, B. Application of Airborne Infrared Remote Sensing to the Study of Ocean Submesoscale Eddies. *Front. Mech. Eng.* **2018**, *4*, 1–10. [CrossRef]
14. Dauhajre, D.P.; McWilliams, J.C.; Renault, L. Nearshore Lagrangian Connectivity: Submesoscale Influence and Resolution Sensitivity. *J. Geophys. Res. Ocean.* **2019**, *124*, 5180–5204. [CrossRef]
15. Dauhajre, D.P.; McWilliams, J.C.; Uchiyama, Y. Submesoscale Coherent Structures on the Continental Shelf. *J. Phys. Oceanogr.* **2017**, *47*, 2949–2976. [CrossRef]
16. Calado, L.; da Silveira, I.; Gangopadhyay, A.; de Castro, B. Eddy-induced upwelling off Cape São Tomé (22° S, Brazil). *Cont. Shelf Res.* **2010**, *30*, 1181–1188. [CrossRef]
17. Castelao, R.M.; Barth, J.A. Upwelling around Cabo Frio, Brazil: The importance of wind stress curl. *Geophys. Res. Lett.* **2006**, *33*, L03602. [CrossRef]
18. Rodrigues, R.R.; Lorenzzetti, J.A. A numerical study of the effects of bottom topography and coastline geometry on the Southeast Brazilian coastal upwelling. *Cont. Shelf Res.* **2001**, *21*, 371–394. [CrossRef]

19. Namiki, C.; Katsuragawa, M.; Napolitano, D.C.; de Lourdes Zani-Teixeira, M.; de Mattos, R.A.; da Silveira, I.C.A. Hydrodynamically-driven distribution of lanternfish larvae in the Southeast Brazilian Bight. *J. Mar. Syst.* **2017**, *170*, 115–133. [CrossRef]
20. Calado, L.; Gangopadhyay, A.; da Silveira, I. Feature-oriented regional modeling and simulations (FORMS) for the western South Atlantic: Southeastern Brazil region. *Ocean. Model.* **2008**, *25*, 48–64. [CrossRef]
21. Silveira, I.; Calado, L.; Castro, B.; Lima, J.; Mascarenhas, A. On the baroclinic structure of the Brazil Current-intermediate western boundary current system. *Geophys. Res. Lett.* **2004**, *31*, L14308. [CrossRef]
22. Castro, B.M.; Lee, T.N. Wind-forced sea level variability on the southeast Brazilian shelf. *J. Geophys. Res.* **1995**, *100*, 16045. [CrossRef]
23. Cerda, C.; Castro, B.M. Hydrographic climatology of South Brazil Bight shelf waters between Sao Sebastiao (24° S) and Cabo Sao Tome (22° S). *Cont. Shelf Res.* **2014**, *89*, 5–14. [CrossRef]
24. Brandini, F.P.; Tura, P.M.; Santos, P.P. Ecosystem responses to biogeochemical fronts in the South Brazil Bight. *Prog. Oceanogr.* **2018**, *164*, 52–62. [CrossRef]
25. Napolitano, D.C.; da Silveira, I.C.A.; Rocha, C.B.; Flierl, G.R.; Calil, P.H.R.; Martins, R.P. On the Steadiness and Instability of the Intermediate Western Boundary Current between 24° S and 18° S. *J. Phys. Oceanogr.* **2019**, *49*, 3127–3143. doi:10.1175/jpo-d-19-0011.1. [CrossRef]
26. Napolitano, D.C.; da Silveira, I.C.A.; Tandon, A.; Calil, P.H.R. Submesoscale phenomena due to the Brazil Current crossing of the Vitória-Trindade Ridge. *J. Geophys. Res. Ocean.* **2020**. [CrossRef]
27. Lazaneo, C.Z.; Napolitano, D.C.; Silveira, I.C.A.; Tandon, A.; MacDonald, D.G.; Ávila, R.A.; Calil, P.H.R. On the Role of Turbulent Mixing Produced by Vertical Shear Between the Brazil Current and the Intermediate Western Boundary Current. *J. Geophys. Res. Ocean.* **2020**, *125*. [CrossRef]
28. Castro, B.M. Summer/winter stratification variability in the central part of the South Brazil Bight. *Cont. Shelf Res.* **2014**, *89*, 15–23. [CrossRef]
29. Rocha, C.B.; da Silveira, I.C.A.; Castro, B.M.; Lima, J.A.M. Vertical structure, energetics, and dynamics of the Brazil Current System at 22° S-28° S. *J. Geophys. Res. Ocean.* **2014**, *119*, 52–69. [CrossRef]
30. Palóczy, A.; da Silveira, I.; Castro, B.; Calado, L. Coastal upwelling off Cape São Tomé (22$^{/}$ *circ*S, Brazil): The supporting role of deep ocean processes. *Cont. Shelf Res.* **2014**, *89*, 38–50. [CrossRef]
31. Carton, J.A.; Chepurin, G.A.; Chen, L. SODA3: A New Ocean Climate Reanalysis. *J. Clim.* **2018**, *31*, 6967–6983. doi:10.1175/jcli-d-18-0149.1. [CrossRef]
32. Egbert, G.D.; Erofeeva, S.Y. Efficient Inverse Modeling of Barotropic Ocean Tides. *J. Atmos. Ocean. Technol.* **2002**, *19*, 183–204. [CrossRef]
33. Large, W.G.; McWilliams, J.C.; Doney, S.C. Oceanic vertical mixing: A review and a model with nonlocal boundary layer parameterization. *Rev. Geophys.* **1994**, *1994*, 363–403. [CrossRef]
34. Durski, S.M.; Glenn, S.M.; Haidvogel, D.B. Vertical mixing schemes in the coastal ocean: Comparison of the level 2.5 Mellor-Yamada scheme with an enhanced version of the K profile parameterization. *J. Geophys. Res.* **2004**, *109*, C01015. [CrossRef]
35. Shcherbina, A.Y.; D'Asaro, E.A.; Lee, C.M.; Klymak, J.M.; Molemaker, M.J.; McWilliams, J.C. Statistics of vertical vorticity, divergence, and strain in a developed submesoscale turbulence field. *Geophys. Res. Lett.* **2013**, *40*, 4706–4711. [CrossRef]
36. McWilliams, J.C.; Gula, J.; Molemaker, M.J.; Renault, L.; Shchepetkin, A.F. Filament frontogenesis by boundary layer turbulence. *J. Phys. Oceanogr.* **2015**, *45*, 1988–2005. [CrossRef]
37. Gula, J.; Molemaker, M.J.; McWilliams, J.C. Submesoscale cold filaments in the Gulf Stream. *J. Phys. Oceanogr.* **2014**, *44*, 2617–2643. [CrossRef]
38. Pereira, F.; Bouali, M.; Polito, P.; da Silveira, I.; Candella, R. Discrepancies between satellite-derived and in situ SST data in the Cape Frio Upwelling System, Southeastern Brazil (23° S). *Remote Sens. Lett.* **2020**, *11*, 555–562. [CrossRef]
39. Brink, K. The near-surface dynamics of coastal upwelling. *Prog. Oceanogr.* **1983**, *12*, 223–257. [CrossRef]
40. Mano, M.F.; Paiva, A.M.; Torres, A.R., Jr.; Coutinho, A.L. Energy flux to a cyclonic eddy off Cabo Frio, Brazil. *J. Phys. Oceanogr.* **2009**, *39*, 2999–3010. [CrossRef]
41. Gula, J.; Molemaker, M.J.; McWilliams, J.C. Submesoscale dynamics of a Gulf Stream frontal eddy in the South Atlantic Bight. *J. Phys. Oceanogr.* **2016**, *46*, 305–325. [CrossRef]
42. Harrison, D.; Robinson, A. Energy analysis of open regions of turbulent flows? Mean eddy energetics of a numerical ocean circulation experiment. *Dyn. Atmos. Ocean.* **1978**, *2*, 185–211. [CrossRef]
43. Lopes, R.M.; Katsuragawa, M.; Dias, J.F.; Montú, M.A.; Muelbert, J.H.; Gorri, C.; Brandini, F.P. Zooplankton and ichthyoplankton distribution on the southern Brazilian shelf: An overview. *Sci. Mar.* **2006**, *70*, 189–202. [CrossRef]
44. De Léo, F.C.; Pires-Vanin, A.M.S. Benthic megafauna communities under the influence of the South Atlantic Central Water intrusion onto the Brazilian SE shelf: A comparison between an upwelling and a non-upwelling ecosystem. *J. Mar. Syst.* **2006**, *60*, 268–284. [CrossRef]
45. Sumida, P.; Yoshinaga, M.; Ciotti, Á.; Gaeta, S. Benthic response to upwelling events off the SE Brazilian coast. *Mar. Ecol. Prog. Ser.* **2005**, *291*, 35–42. [CrossRef]
46. Dritschel, D.G.; Haynes, P.H.; Juckes, M.N.; Shepherd, T.G. The stability of a two-dimensional vorticity filament under uniform strain. *J. Fluid Mech.* **1991**, *230*, 647–665. [CrossRef]

47. Parker, D.J. Barotropic instability in frontolytic strain. *Q. J. R. Meteorol. Soc.* **1998**, *124*, 1617–1632. [CrossRef]
48. Brink, K.H. Continental Shelf Baroclinic Instability. Part I: Relaxation from Upwelling or Downwelling. *J. Phys. Oceanogr.* **2016**, *46*, 551–568. [CrossRef]
49. Brink, K.H.; Seo, H. Continental Shelf Baroclinic Instability. Part II: Oscillating Wind Forcing. *J. Phys. Oceanogr.* **2016**, *46*, 569–582. [CrossRef]
50. Campos, E.J.D.; Gonçalves, J.E.; Ikeda, Y. Water mass characteristics and geostrophic circulation in the South Brazil Bight: Summer of 1991. *J. Geophys. Res.* **1995**, *100*, 18537. [CrossRef]
51. Palma, E.D.; Matano, R.P. Disentangling the upwelling mechanisms of the South Brazil Bight. *Cont. Shelf Res.* **2009**, *29*, 1525–1534. [CrossRef]